PHS1-mediated microtubule depolymerization in *Chlamydomonas reinhardtii*

Ng Lee Mei

Nara Institute of Science and Technology

Graduate School of Biological Sciences

Plant Cell Function Lab
Prof. Takashi Hashimoto

Contents

INTRODUCTION

Stress response and adaptation in plant evolution

All organisms including human, animals, plants and microbes have their own mechanisms to cope with environmental stresses, regardless of abiotic or biotic. Abiotic stresses such as temperature, salinity and drought are few of the common environmental stresses faced by plants. Plant growth is stopped or retarded under the environments unfavorable for optimal growth. This growth retardation is a positive response; upon perception of stress, plants activate signaling pathways that culminate in inhibition of cell division or cell expansion. Molecular mechanisms of stress-induced growth retardation are not fully understood. Since plants are sessile, in order to adapt and survive through harsh environments, plants need to regulate biochemical and metabolic activities, gene expression patterns, growth and developmental decisions. These regulations are important to enable plants to adapt and survive by way of restoring cellular homeostasis (Xiong and Zhu, 2002; Zhu, 2002; Vinocur and Altman, 2005).

Development of new gene functions and novel or rewired signaling pathways is one way that may help plants to have sustainable growth, survival and adaptation towards environmental stresses. Evolution is an important natural event taking place on earth, where all species are associated. It is a natural selection process, where species with genes that are best suited to its growth and survival is conserved and passed down to the next generations. Non-essential genes may be lost. For example, a recent study on genome wide analyses in 2511 chloroplast genomes revealed that chloroplast genes such as *PsaM*, *Psb30*, *ChlB*, *CHIL*, *CHIN* and *RPL32* are present in algae, bryophytes, pteridophytes and gymnosperms but not in angiosperm (Mohanta et al., 2020).

The plant evolution timeline reveals that algae are located at the basal lineage of the plant evolution and algae have been regarded as the ancestor of the plant kingdom (Wodniok et al., 2011) (Figure 1). The unicellular algae group includes red algae, brown algae and green algae. The first land plant evolved from green algae approximately 510 million years ago, advanced from unicellular to multicellular organizations, in which liverworts, hornworts and mosses are the few known examples of early land plant lineages. The evolution continues to the emergence of vascular plants, ferns, non-flowering gymnosperms, and finally flowering angiosperms. The complexity of organisms varies as it is evolving; the process of plant adaptation towards environmental stresses proceeds with modifications in tissue or organ structures, and signaling and metabolic pathways.

Land plants tend to evolve and develop more complex signaling pathways which form a network of regulatory genes with integrations of positive and negative interactions. For example, a calcium signaling pathway involves stress response, cell cycle progression, positive and negative regulatory genes, and interactions with other signaling pathways such as sucrose signaling pathways (Tuteja and Mahajan, 2007). Among several land plant-specific growth regulators in response to environmental stresses, as representative examples, I will here summarize functions of ABA, DELLA, and SOG1.

Abscisic acid (ABA) controls plant growth and development such as leaf abscission and fruit ripening. It also acts as stress hormone when plants encounter various abiotic stress conditions (Sagee et al., 1980; Chernys et al., 2000). During drought and salt stresses, ABA level is elevated in plants, resulting in turgor pressure decrease in guard cells and closure of stomata (Suzuki et al., 2013). Closure of stomata reduces water loss from plants and thereby enhances stress tolerance. A series of core components including PYRs, Group A PP2C, SnRK2s, ABFs, AFPs, PDRs, ABCG25 and AITs are needed for a functional ABA signaling pathway. Although several core component homologues of ABA response were found in algae, the complete core components of the ABA signaling pathways only emerged in early land plants such as *Marchantia polymorpha* (Wang et al., 2015)(Figure1), as AFPs and ABA receptor PYR proteins are only found in land plants.

Under stress conditions, DELLA proteins integrate various plant hormone pathways, such as auxin and jasmonic acid, and negatively regulate plant growth by restraining cell proliferation and expansion (Achard et al., 2006; Achard et al., 2009; Gao et al., 2011). DELLA proteins were initially characterized as GA repressors (Peng et al., 1997; Hauvermale et al., 2012; Claeys et al., 2014). Although DELLA proteins repress plant growth in harsh environments, it is advantageous to plants where they promote and enhance plant survival (Achard et al., 2006). Interaction and development of the GA-GID-1-DELLA signaling patheay occurs after bryophyte divergence whereas DELLA-mediated growth repression occurs before or after fern divergence (Yasumura et al., 2007; Sun, 2011).

Plants efficiently stop cell division when exposed to high dosages of ultra-violet light or chemicals that damage plant genomes (Sakamoto et al., 2011; Nezames et al., 2012; Sjogren et al., 2015). Suppressor of Gamma Response 1 (SOG1), a plant-specific transcription factor, is immediately activated, possibly by phosphorylation upon DNA damage, and regulates expression

of many genes involved in cell cycle arrest, DNA repair and programmed cell death (Yoshiyama et al., 2009; Yoshiyama et al., 2014; Yoshiyama, 2015). In *Arabidopsis sog1*mutants, seedling roots keep growing when challenged with DNA damage-causing chemicals, while root growth in wild-type seedlings are effectively inhibited (Yoshiyama et al., 2014). SOG1 is absent in algae but has been identified in moss (*Physcomitrlla patens*), gymnosperms and angiosperms, indicating that SOG1 has evolved in early land plants to cope with DNA-damaging radiation (Yoshiyama et al., 2014)(Figure 1).

Microtubules

In all eukaryotic cells, microtubules support a variety of cellular functions in cells, including cell division, intracellular transportation, cell motility, and polar cell expansion. Microtubule is a hollow-shaped cytoskeletal polymer, comprised of 13 protofilaments with heterodimers of α- and β-tubulin that are arranged in parallel (Figure 2). These long and thin protofilaments have two distinct polar ends, designated as a fast growing plus-end (+) and a slow growing minus-end (–). The presence of microtubule polarity is essential in determining the direction of cellular cargo movement by microtubule motor proteins (Robinson et al., 1995).

In microtubules, tubulin dimers assemble and disassemble from the plus-end of the protofilaments continuously, resulting a phenomenon called dynamic instability (Mitchison and Kirschner, 1984). The tubulins containing GTP-bound β-tubulin polymerize at the plus end. However, hydrolysis of GTP to GDP weakens the tubulin binding affinity for adjacent molecules, resulting in depolymerization of microtubules. The GDP-tubulin molecules which disassociate from the protofilaments are replaced with the GTP-tubulin molecules in the cytoplasm. This continuous association and disassociation of tubulin molecules results in the growth and shrinkage of microtubules (Mitchison and Kirschner, 1984; Erickson and O'Brien, 1992; Cassimeris, 1993). The microtubule dynamics depends on the rate of tubulin addition and GTP hydrolysis, where the tubulin bound GTP is necessary to maintain microtubule stability (Carlier et al., 1984). If the rate of the GTP-tubulin is faster than the rate of GTP hydrolysis, the more tubulin molecules retain at the plus end of microtubules, and hence microtubules grow.

Acetylation is one of the common post-translational modifications of tubulins which occurs by transfer an acetyl moiety from acetyl-coenzyme A to the side chain of the lysine residue at position 40 (Lys40) of α-tubulin (L'Hernault and Rosenbaum, 1985; LeDizet and Piperno, 1986;

Li and Yang, 2015). Acetylation in α-tubulin has been termed synonymy as 'stable microtubule' due to its close association with unusually stable microtubules (Janke and Bulinski, 2011, Al-Bassam and Corbett, 2012). A structural modeling study proposes that the acetylation may stabilize lateral interactions between neighboring tubulin protofilaments (Cueva et al., 2012). Acetylation occurs on long-lived cytoplasmic microtubules with slow dynamics that are resistant to depolymerization (Webster and Birisy, 1989). By using antibody specific for the acetylated tubulin, acetylated tubulin is found in cilia, flagella, basal bodies, centrioles and microtubules in the mitotic spindle (Piperno and Fuller, 1985, Piperno et al., 1987).

A wide variety of drugs are reported to have effects on microtubules stability. Microtubule stabilizing drug taxol stabilizes the microtubules by binding to the β-tubulin, increases acetylation level and promotes microtubule polymerization, whereas microtubule destabilizing drugs such as vinblastine, propyzamide, oryzalin and colchicine inhibit the microtubule assembly by binding to the tubulin dimers or polymerized form of microtubules (Schiff et al., 1979; Toso et al., 1993; Jordan and Wilson; 2004; Xiao et al., 2006). Although these two types of drugs affect microtubules stability differently, they are altogether regarded as anti-mitotic agents, which eventually inhibit cell proliferation by halting mitosis during cell division (Jordan and Wilson, 2004). These drugs have facilitated the studies on microtubule function and assembly or microtubule-dependent processes in many organisms (Schibler and Huang, 1991; Naoi and Hashimoto, 2004; Van Damme et al.,2004).

Besides experimental application of drugs, the stability of microtubules is also challenged by external stimuli such as abiotic stresses. Microtubules disruption occurs under salt and osmotic stresses and results in right-handed skewed growth of *Arabidopsis* seedling roots (Wang et al., 2007; Fujita et al., 2013). High levels of stress induce rapid microtubule depolymerization and reorganization into a new microtubule network. The reorganization of microtubules is proposed to be important to enhance salt tolerance in plants (Wang et al., 2007).

Microtubules are essential in mitosis and cell division by adopting several distinct arrays during the cell cycle progression (Goddard et al., 1994; Sugimoto et al., 2000; Hashimoto et al., 2015). During interphase, microtubules arrays are distributed beneath the plasma membrane and are arranged transverse to the elongation axis of the cell during non-dividing interphase. It forms the preprophase band during pre-prophase and progresses to spindle microtubules during metaphase. In anaphase, the kinetochore microtubules are shorten and the newly formed daughter

chromosomes are pulled to the opposite of mother chromosomes. Phragmoplast expands towards the cell cortex and arranges in opposite orientation until cytokinesis completes. Disruption of microtubules by drugs such as taxol or vinblastine halts mitosis and delays cell cycle progression with prolonged mitotic arrest (Jordan et al., 1992; Jordan et al., 1993; Sorger et al., 1997).

Plant growth and development depend on cell expansion. Cortical microtubules form parallel array in the plasma membrane during interphase and plays an important role in directional cell expansion. Microtubule-associated proteins, such as MOR1 and SPIRAL1, affect directional cell expansion in plant cells (Whittington et al., 2001; Nakajima et al., 2004). These proteins affect microtubule organization and their mutations result in unusual plant expansion and elongation.

Propyzamide Hypersensitive 1

Propyzamide Hypersensitive 1 (PHS1) was first reported more than a decade ago (Naoi and Hashimoto, 2004). It was found that *phs1-1d* mutant roots formed left-handed helices in contrast to the wild-type roots which grew straight to the direction of the gravity vector in normal growth conditions. When exposed to 3 mM propyzamide, a microtubule-disrupting drug, cortical microtubules of *phs1-1d* roots were almost completely depolymerized, resulting in radial cell expansion, whereas wild-type root epidermal cells showed partial disruption of cortical microtubules with left-handed twisted growth. The *phs1-1d* mutation is a semi-dominant gain-of-function mutation, while loss-of-function mutations of *PHS1* show no obvious phenotypes in plant growth and morphology under standard growth conditions (Naoi and Hashimoto, 2004; Pytela et al., 2010). *PHS1* is expressed in many cell types but the strong expression is observed in rapidly elongating cells such as etiolated hypocotyls and the root elongation zone (Pytela et al., 2010). PHS1 protein is strongly retained in the cytoplasm by the nuclear extrusion signal (NES) at the C-terminus and by transient associations with endomembranes (Pytela et al., 2010).

PHS1 consists of a kinase domain, which shows homology to the actin-fragmin kinase and a dual-specificity phosphatase domain belonging to the MAP kinase phosphatase family (Fujita et al., 2013). *In vitro* kinase assays showed that α-tubulin was phosphorylated by phosphatase-dead mutant but not kinase-dead mutants, indicating that kinase domain of PHS1 phosphorylates α-tubulin (Fujita et al., 2013). The phosphorylated amino acid residue of α-tubulin was identified at Thr-349 (Fujita et al., 2013; Hotta et al., 2016). The association between kinase and phosphatase in *in vitro* assays had led to a proposed PHS1 activation model (Figure 3) (Fujita et al., 2013, and

unpublished results in the Hashimoto lab). Under normal growth conditions, the phosphatase suppresses the kinase activity, which promotes the polymerization of tubulin. However, under stressed conditions, the phosphatase activity is suppressed, thereby causing phosphorylation at the Thr-349 of α-tubulin, and subsequent depolymerization of microtubules (Fujita et al., 2013). These mechanisms are transient; microtubules are repolymerized shortly even in the presence of continuous stresses.

A conserved kinase interacting motif (KIM) (LVRKR) was identified in *Arabidopsis* PHS1 from sequence alignment of different plant PHS1 homologues (Naoi and Hashimoto, 2010). In the gain-of-function *phs1-1d* mutant, the critical Arg residue in the putative KIM was mutated to Cys. The PHS1^{R64C} mutant protein exhibited partial phosphatase activity compared to the wild-type protein, while the PHS1 mutant protein with a phosphatase catalytic residue C792 showed no phosphatase activity. This demonstrates that the PHS1 phosphatase is an enzymatically active phosphatase and the important role of KIM motif of PHS1 suppressing the phosphatase activity (Naoi and Hashimoto, 2010). Transient expression assays showed that PHS1^{R64C} partial depolymerized cortical microtubules whereas the phosphatase null mutant protein caused complete depolymerization in plant cells (Fujita et al., 2013).

The morphology of *phs1* null alleles were indistinguishable from wild-type plants except that the mutant roots exhibited abnormal growth direction when challenged with low dosages of propyzamide (Pytela et al., 2010). However, the phosphatase-dead *phs1* mutants exhibited radially expanded cells with severe dwarf phenotypes (Fujita et al., 2013). Physiological functions of PHS1 are not known since growth of the *phs1* null mutants even under various stress conditions did not reveal any differences from growth and morphology of wild-type plants (unpublished results in the Hashimoto lab). A *phs1-5* allele was reported to show a late flowering phenotype (Tang et al., 2016) but other *phs1* null alleles, *phs1-4* and *phs1-8,* showed no such flowering phenotypes, indicating that the flowering phenotypes only observed in *phs1-5* may be caused by a second site mutation unrelated to PHS1 (unpublished data in the Hashimoto lab).

Chlamydomonas reinhardtii

Chlamydomonas reinhardtii is a haploid, unicellular, biflagellate, oval-shaped green alga. Plant evolution timeline reveals that *Chlamydomonas* is located at the basal lineage of plant evolution and represents one of the simplest photosynthetic eukaryotes.

A *Chlamydomonas* cell has two anterior flagella that expand out from the basal bodies to enable its motility. The flagella are constructed by nine outer doublet microtubules arrayed around a central pair of singlet tubules, formed a '9 + 2' arrangement (Flavin and Slaughter, 1974) (Figure 4). *Chlamydomonas* has been used in studies of many axonemal and flagellar microtubules as well as the intraflagellar transport machinery (Flavin and Slaughter, 1974; Huang et al., 1979; Johnson, 1998; Meng and Pan, 2016; Harris et al., 2016; Kubo et al., 2018). In addition, acetylation is highly enriched on axonemal tubulin. Therefore, many flagellar regeneration and resorption studies were reported by using antibody specific for acetylated tubulins (Maruta et al., 1986; Mittelmeier et al., 2011).

Basal bodies act as organizing centers for cytoplasmic microtubules and play an important role during cell division. There are two basal bodies in *Chlamydomonas*: mother and daughter basal bodies. A four-member microtubule rootlet and a two-member microtubule rootlet are extended out from each of the basal body in *Chlamydomonas* (Figure 4). These microtubule rootlets are extended along the cell. It is also often associated with acetylated microtubules, indicating their stability (Mittelmeier et al., 2011). Besides the aforementioned axoneme and basal bodies, acetylated tubulins are also present in cytoplasmic microtubules (LeDizet and Piperno, 1986).

Eyespot is generally found in unicellular photosynthetic organisms, including *Chlamydomonas*. It is positioned adjacent to the four-member microtubule rootlet extended from a daughter basal body (Holmes and Dutcher, 1989; Mittelmeier et al., 2011). It is a light-sensing and photoreceptive organelle, which allows it to sense light direction and intensity (Ueki et al., 2016). *Chlamydomonas* cells respond to the light stimulus by swimming towards or away from the light source.

Chlamydomonas has been used as a model organism in many studies due to its short generation time and availability of complete genome sequences including nuclear, chloroplast and mitochondrial genomes (Merchant et al., 2007). A large number of mutant collections are maintained by Chlamydomonas Resource Centre in University of Minnesota. In addition, molecular techniques such as cloning, transformation, microscopy imaging and complementation analysis are also established (Tam et al., 1993; Purton and Rochaix, 1994; Yamano et al., 2012). Synchronization of the *Chlamydomonas* cells can be achieved by culturing them under a designated light and dark regime in a specific culture medium with defined temperatures (Spudich and Sager, 1980; Garz et al, 2012).

Chlamydomonas is easier to handle because it is a haploid, unicellular organism with less complicated genome and shorter generation time compared to land plants. This has made it a good alternative to study functionality of plant-related genes. A well annotated complete chloroplast and nuclear genomes and its capability to grow heterotrophically solely depending on acetate as sole carbon source in the dark has made *Chlamydomonas* becomes a useful model organism in chloroplast biogenesis and photosynthetic and non-photosynthetic mutational studies (Heifetz et al., 2000; Ramundo et al., 2013, Minai et al., 2006).

Chlamydomonas also has been used in stress-related studies, such as microtubule dynamics in acidic and saline conditions, construction of an engineered salt-resistant strains, and adaptation to cold stress (Valledor et al., 2013; Liu et al., 2017; Kato et al., 2017). Enlarged cell size, disturbed cell division and formation of palmelloids were observed in stressed conditions (Neelam and Subramanyam, 2013; Ermilova, 2020). Flagella were resorbed after high Na^+ stresses causing motility loss (Neelam and Subramanyam, 2013).

Chlamydomonas **cell cycle**

The *Chlamydomonas* cell cycle consists of a long G1 phase (interphase) and a short S/M phase, which involves in DNA replication and segregation. In G1-S/M phase, more than 4,000 genes function in cell division, basal body and cell wall processes (Tulin and Cross, 2015). Cell cycle genes such as cyclin-dependent kinases (CDKs), cyclins (CYCs) and regulatory proteins/transcription factors are involved in the cell cycle transcriptional changes by initiating or promoting different cell cycle events. For example, CDKA is required to initiate S/M cell cycle, whereas CDKB is needed for DNA replication during mitosis. Three main classes of cyclins families, A, B and D-types, are also important regulators in the cell cycle. For example, A- and B-type cyclins regulate the S phase and mitosis, respectively (Bisova et al., 2005).

Chlamydomonas cells divide by multiple fission (Figure 5). During the G1 phase, a cell grows by expanding its cell size. It enters the S/M phase when the cell reaches its minimum critical size. Rapid alternation between the S phase and mitosis allows DNA replication to occur and produce 2^n daughter cells, where 'n' is the doubling number of daughter cells. Cell division number is higher if a mother cell is in optimum conditions. One complete cell cycle takes about 30 min (Cross and Umen, 2015). The initial daughter cells are in a clumped form, known as pamelloid, where the cells are waiting to be hatched and separated. At the end of S/M phase, daughter cells

are released from the mother cells by producing 2^n daughter cells, i.e. 2, 4, 8 or 16 daughter cells depending on the number of cell division. New cell cycle progression continues in daughter cells by starting a new G1 phase.

A typical diurnal cycle regulating light and dark periods is frequently used to synchronize *Chlamydomonas* cells, where the G1 phase occurs during the light period and the S/M phase in the dark period. *Chlamydomonas* cell cycle progression is growth-dependent. Longer light period allows a cell to grow bigger before it enters mitosis. A *Chlamydomonas* cell can grow more than 10-fold in size if the G1 phase lasts for 10 to 14 hours (Cross and Umen, 2015).

Microtubules form distinct arrays in different phases of the cell cycle (Figure 6) (Cross and Umen, 2015). During interphase, flagella and stable microtubule rootlets extend out from basal bodies. In prophase, flagella are shortened and retracted. Basal bodies replicate by forming pro-basal bodies. During metaphase, the pro-basal bodies are elongated. It is drawn to the opposite sides of the cell, the spindle pole. Then, chromosomes start condensation and spindle microtubules enter the nucleus and attach to the chromosomes. A metaphase band of microtubules emerges at the future plane of cytokinesis. After cytokinesis, flagella re-grow.

In my thesis, I studied hyperosmotic stress-induced microtubule destabilization in *Chlamydomonas reinhardtii*. *Chlamydomonas* PHS1 triggers rapid and transient tubulin phosphorylation, which results in microtubule destabilization in interphase and mitosis. My results complement what is known in previous studies from *Arabidopsis* plants, and provide future useful insights into future research to elucidate physiological functions of PHS1.

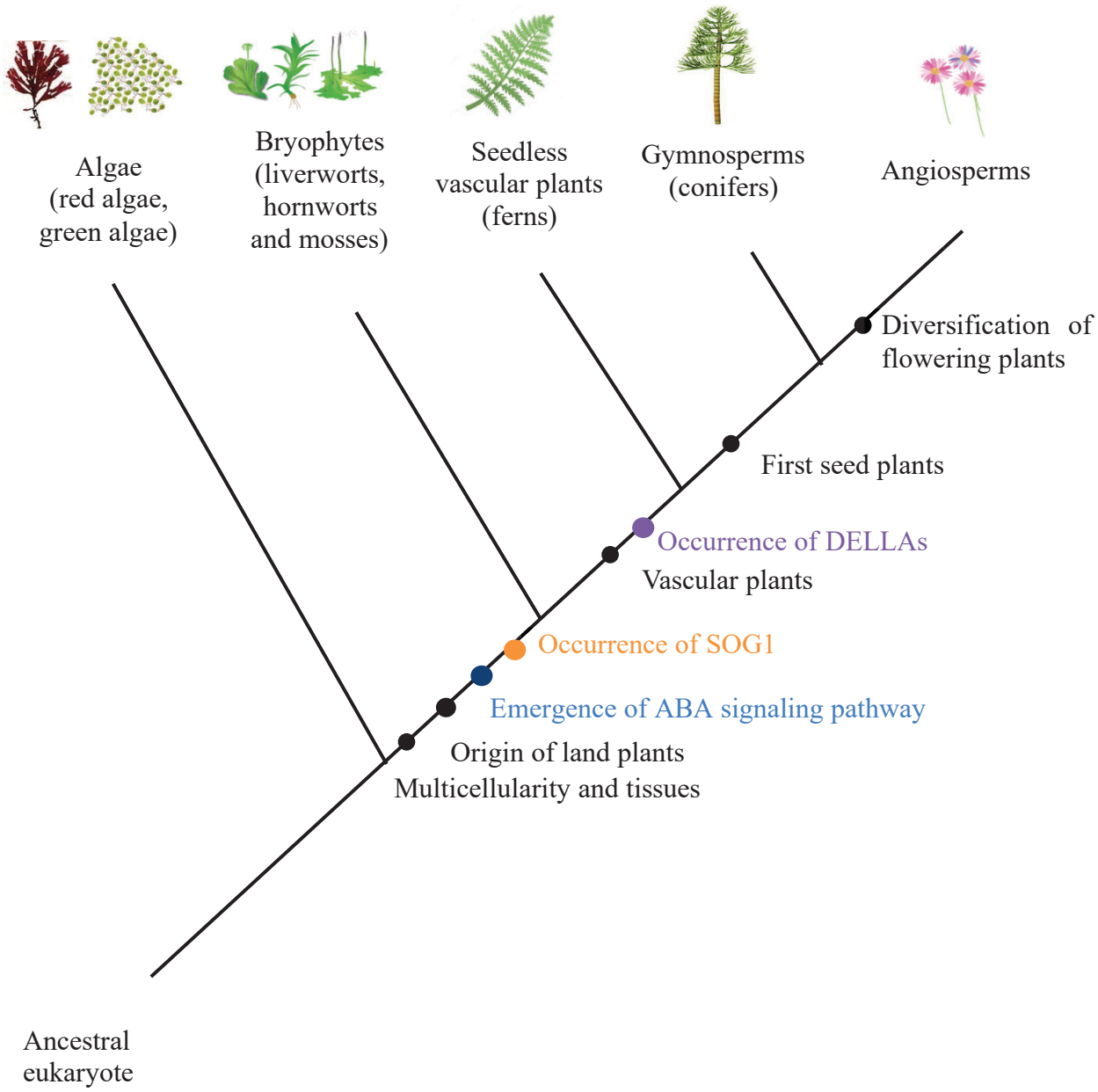

Figure 1: The evolution of plants, from algae to angiosperms. The black dots are selected plant features that have emerged during evolution; the blue dot indicates the emergence of ABA signaling pathway; the orange dot indicates the occurrence of SOG1; the purple dot indicates the occurrence of DELLAs.

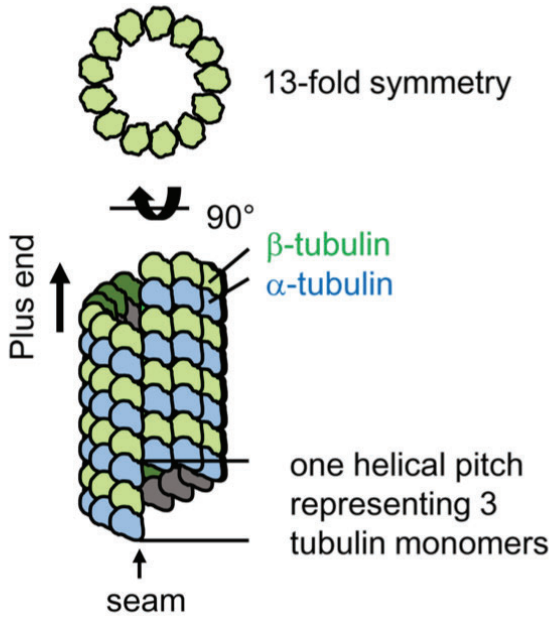

Figure 2: The structure of microtubules (Hashimoto, 2015). Protofilaments are composed of a stacked heterodimers of α- and β-tubulins that are arranged in parallel. These 13 protofilaments laterally associate and form a hollow-shaped tube.

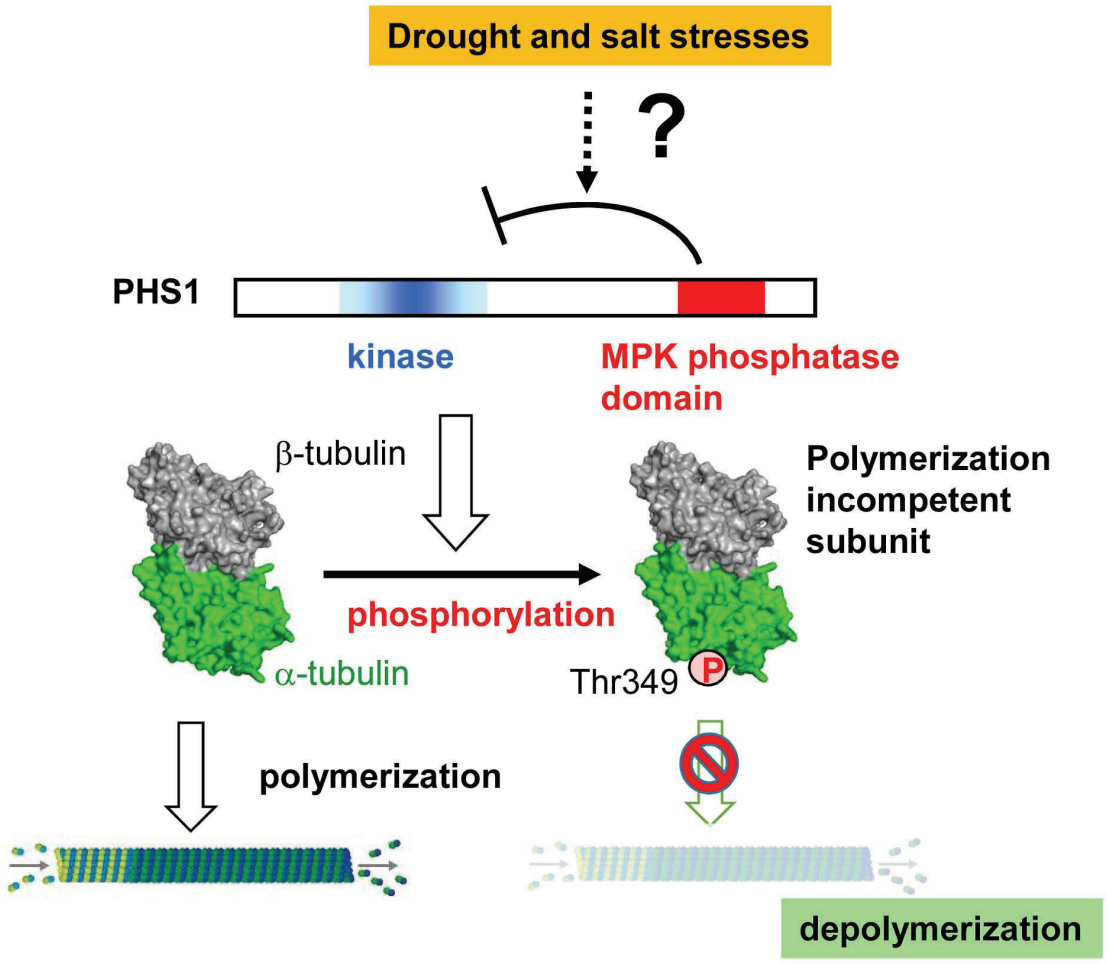

Figure 3: The working model of PHS1 under normal and stressed conditions (Fujita et al., 2013 and unpublished data). Under non-stressed conditions, tubulin kinase activity is suppressed by the MAP kinase phosphatase-like domain in PHS1. The phosphatase is postulated to de-phosphorylate an active-site residue (or residues). Drought and salt stresses activate the tubulin kinase, possibly by inactivating the phosphatase activity. Activated kinase phosphorylates the Thr349 of α-tubulin and results in destabilization (or depolymerization) of microtubules.

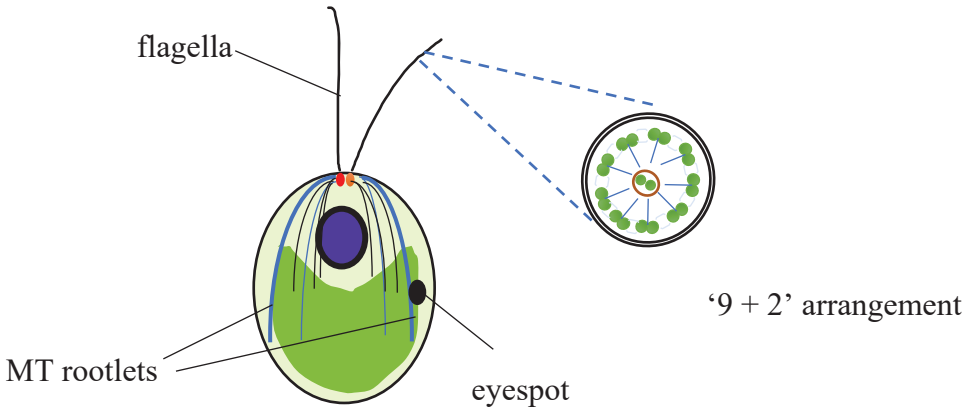

Figure 4: *Chlamydomonas reinhardtii*. Flagella are constructed by nine outer doublet microtubules arrayed around a central pair of singlet tubules, forming a '9 + 2' arrangement. Flagella are extended out from mother (red oval) and daughter (orange oval) basal bodies. A four-member microtubule rootlet (thick blue lines) and a two-member microtubule rootlet (blue thin lines) are extended from each basal bodies. Microtubule network in the cell body is shown by black thin lines. Black oval indicates eyespot in *Chlamydomonas* positioned along a four-member microtubule rootlet extending from a daughter basal body.

Figure 5: *Chlamydomonas* multiple-fission cell cycle. *Chlamydomonas* has a long G1 phase during which a cell expands to a critical cell mass. Then, falagella are adsorbed into the cell, which divides n times successively without a G2 phase. After cytokinesis, daughter cells remain clustered in a palmelloid, until it hatches to release new daughter cells.

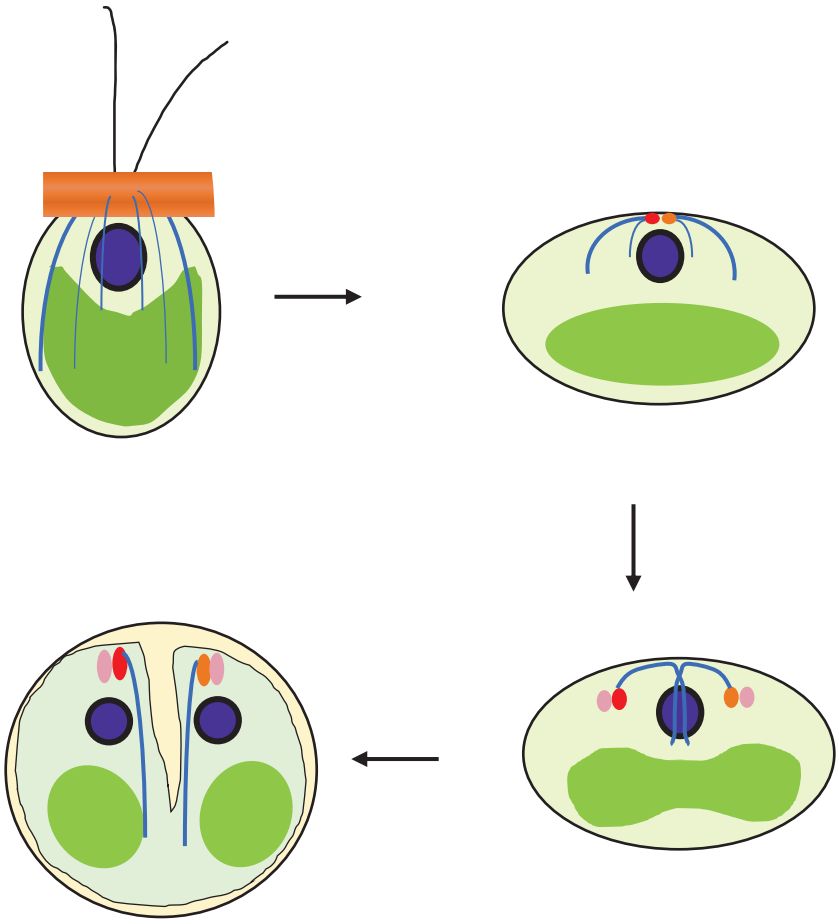

Figure 6: Microtubules in a simple *Chlamydomonas* cell division model (modified from Cross and Umen, 2015). Shown in the figure are four-member microtubule rootlets (thick blue lines), two-member microtubule rootlets (blue thin lines), basal bodies (red and orange ovals), pro-basal bodies (pink ovals), chloroplasts (green circles), and nuclei (purple circles).

MATERIALS AND METHODS

Strains, media and culturing conditions

C. reinhardtii wild-type strain CC-4533 (Jonikas cMJ030), LMJ.RY0402.157476.1 (*phs1-1*), LMJ.RY0402.181368 (*phs1-2*), and LMJ.RY0402.163064 (*phs1-3*) were purchased from Chlamydomonas Library Project (Li et al., 2016). All strains were maintained and cultured in Tris-acetate-phosphate (TAP) medium (0.4 g/L NH_4Cl, 0.1 g/L $MgSO_4 \cdot 7H_2O$, 0.05 g/L $CaCl_2 \cdot 2H_2O$, 0.108 g/L K_2HPO_4. 0.056 g/L KH_2PO_4, 2.42 g/L Tris, 1 mL/L glacial acetic acid, 5 mg/L $Na_2 \cdot EDTA$, 2.2 mg/L $ZnSO_4 \cdot 7H_2O$. 1.14 mg/L H_3BO_3, 5.1 mg/L $MnCl_2 \cdot 4H_2O$, 0.5 mg/L $FeSO_4 \cdot 7H_2O$, 0.16 mg/L $CoCl_2 \cdot 6H_2O$, 0.16 mg/L $CuSO_4 \cdot 5H_2O$, 0.11 mg/L $(NH_4)_6Mo_7O_{24} \cdot 4H_2O$ and 1.6 mg/L KOH) (Gorman & Levine, 1965).

To synchronize cell growth, *Chlamydomonas* cells were grown in 25 mL of the TAP liquid medium with horizontal shaking at 100 rpm in an incubator shaker (Sanki) under white light (16,000 lux) with light : dark (12 hour:12 hour) photoperiod. Every day cells were diluted to OD_{750} = 0.05 at the beginning of the light regime. The temperature in the incubator shaker was 26°C during illumination and 22°C during the dark regime.

Sequence identification and phylogenetic analysis of *PHS1* gene in algae and plants

Arabidopsis thaliana PHS1 protein (NP_851066.2) was used as the query sequence against the plant genome with complete genome sequence deposited in Phytozome, Phycocosm, ConGenIE database and GenBank at National Center for Biotechnology Information (NCBI). A *PHS1* gene was identified with two criteria: (a) a tubulin kinase domain (which contains three catalytically critical amino acid residues, K187, D309, and N324) juxtaposed with a MAP kinase phosphatase domain in a single ORF, (b) confidence value/Expect (E)-value less than e^{-10}.

Kinase-domain sequences of 15 PHS1 proteins were aligned using the ClustalW algorism. The phylogenetic tree was construct by the maximum likelihood method using MEGA X (Kumar et al. 2018). The confidence level of each branch was estimated by 500 bootstrap replications.

Stress treatment

Stock solutions for 3 M NaCl, 3 M sorbitol and 10 mM propyzamide (Wako) were prepared for stress treatment in *Chlamydomonas*. Final concentration of DMSO does not exceed 0.05% of the

total culture volume in each experiment. A commercial seawater mixture (GEX) was purchased and prepared by adding 25 g in 1 L MiliQ water.

For preliminary experiment using seawater, salt and sorbitol (Figure 9, 10, 12 and 14), the corresponding volume of seawater, salt or sorbitol was applied to asynchronous *Chlamydomonas* cells, and cultured under continuous light for 20 min with a final volume of 50 mL.

Stress treatment for interphase and mitotic phase experiments (Figure 18, 20, 21, 22) were performed at the 6^{th} hr (interphase) and at the 11^{th} hr from the beginning of the light period (mitotic), respectively. For continuous stress treatment experiments, sorbitol or propyzamide treatment applied to the cells at the beginning of the light period (Figure 25, 27 and 28). For stress treatment before mitotic phase starts experiments (Figure 26 and 29), sorbitol or propyzamide was applied at the 9^{th} hr from the light period. To begin stress treatment experiment, approximately 2 x 10^5 of freshly cultured *Chlamydomonas* cells were directly transferred to a new flask. Fresh TAP culture medium was topped up when necessary. Lastly, sorbitol or propyzamide was added into the culture medium to obtain a final volume of 25 mL.

Cell number and cell size analysis

The Z2 Coulter Particle Count and Size Analyzer (Beckman Coulter) was used to measure the number of cells and the cell volume. When cells form aggregates (palmelloids), the number of palmelloids (but not the individual cells in the palmelloids) was counted. *Chlamydomonas* cells (100 μL) were first fixed with 1% glutaraldehyde and then immediately mixed with 10 mL of coulter isoton diluent (Beckman Coulter). The cell size range was set between 60 to 3400 μm^3. Data was exported using Coulter (R) Z2 AccuComp(R).

Growth rate of *Chlamydomonas* cells were calculated. Statistical significance between the means of groups was calculated by one-way ANOVA (Analysis of Variance) with Tukey HSD (Tukey Honest Significant Differences) post-hoc test, where p-value <0.05 indicates significantly different. This analysis was performed using R statistical software ver3.6.3.

Plasmid construction

To generate a plasmid for genetic complementation, a hygromycin selectable marker expression cassette (Berthold et al., 2002) was cloned between the *EcoR*V and *Kpn*I sites of *pBluescript II KS* (+) plasmid. Then, a genomic fragment of *PHS1* (11,063 bp) was released from the fosmid clone

(GCRFno27_g18 from the *C. reinhardtii* C9 strain) by digestion with *Hind*III and cloned into the *Hind*III site of the *pBluescript II KS* (+) plasmid described above to generate pgCrPHS1.

Transformation of the *PHS1* gene into *phs1-2*

Transformation was performed according to a published method (Yamano et al., 2012) with some modifications. Fresh overnight culture of *Chlamydomonas* cells were centrifuged at 600 x *g* for 5 min and washed twice with 10 mL of MAX Efficiency Transformation Reagent for Algae (Invitrogen). The 1 x10^8 cells and approximately 1 μg of the *XbaI*-restricted pgCrPHS1 plasmid were mixed and then transferred to an electroporation cuvette. After incubation for 5 min at 4°C, a single electric pulse with voltage of 0.4 kV for about 4s was applied using MicroPulser™ (Bio-Rad). Electroporated cells were transferred to 10 mL of TAP medium containing 40 mM sucrose and were grown under dim light overnight. The cells were then spread onto TAP agar plate containing 30 μg/mL hygromycin, and grown for 5 days. Putative transformants were picked and checked by genomic PCR analysis.

DNA extraction and polymerase chain reaction (PCR)

Chlamydomonas cells grown on a TAP agar plate were mixed well in 50 μL of 5% Chelex (Invitrogen) and were vortexed for 15 s before subjected to 100°C for 10 min. The tube was then placed on ice for 1 min and centrifuged at 12,000 rpm for 2 min. The supernatant was transferred to a new tube and was used for PCR analysis. Each sample contained a final concentration of 1 x PCR buffer for KOD FX Neo, 0.4 mM dNTP, 0.2 μM PCR forward and reverse primers, 0.5 μL KOD FX Neo, 0.5 μL of DNA template, and sterile MiliQ water to fill up to 25 μL. PCR conditions: 95°C for 5 min; followed by 30 cycles of 95°C for 5 s, 58°C for 45 s and 72°C for 1 min; finally 72°C for 2 min. The primers sequences: PHS1_P1, 5'-CACACATAGGTGACAATGGGACAC-3', PHS1_P2, 5'-GCAGCAGTAGCAACATAAGCAGTA-3' and LB, 5'-TGGGCGCCGTAGTTAAGACAAA-3'.

Quantitative reverse-transcription PCR

Chlamydomonas cells were harvested by centrifugation at 600 x *g* for 5 min and disrupted by mortar and pestle with liquid nitrogen. Total RNA was extracted by using RNeasy Mini kit (Invitrogen) according to the manufacturer's instructions. Cell homogenates were mixed with 450

μL of the RLT buffer and transferred to a QIA shredder spin column. After centrifugation, the flow-through fraction was collected and 225 μL of 100% ethanol was added. The mixture was transferred to a RNeasy spin column. After centrifugation at 8,000 x *g* for 15 s, 700 μL of RW1 buffer was added to the column and subjected to centrifugation at 8,000 x *g* for 15 s. The flow-through fraction was discarded. A total of 500 μL RPE buffer was added to the column and again centrifuged at 8,000 x *g* for 15 s. This step was repeated using 500 μL RPE buffer but with centrifugation for 2 min. The column was carefully transfer to a new 1.5-mL centrifuge tube. Finally, 30 μL of RNase free water was added into the column and centrifuged at 10,000 x *g* for 1 min and kept at – 80°C.

ReverTraAce®qPCR MasterMix with gDNA remover (Toyobo) was used to reverse transcript RNA. A total of 0.5 μg of RNA was used per reaction. All samples were heated to 65°C for 5 min and transferred to ice immediately. Then, 4 x DN master mix was added. After the samples were incubated for 37°C for 5 min, 5 x RT master mix was added into the reaction mixture and then subjected for incubation: 37°C for 15 min, 50°C 5 min, 98°C for 5 min. The cDNA was kept at – 20°C.

RT-qPCR was performed using Light Cycler 96 (Roche) with TB Green™ *Premix Ex Taq*™ II (Takara). Each sample consists of a final concentration of 1 x TB Green Premix Ex Taq II, 0.4 μM of PCR forward and reverse primers and 1 μL of cDNA template top up to 10 μL. The thermal program was 95°C for 30 s (initial denaturation); followed with 40 cycles of 95°C for 5 s and 60°C for 30 s; 1 cycle of 95°C for 5 s, 60°C for 1 min (melting); finally 50°C for 30 s (cooling). A sodium/phosphate symporter gene (*PTB-1)* was used as a reference gene. Primers sequences for qPCR: PTB1-F, 5'-GCCTACTCGCCCAGCATC-3', and PTB1-R, 5'-TGTTGGTGCGGTTGAGCA-3'; CDKB-F, 5'-ACCTGCACCGCATCTTCC-3', and CDKB-R 5'-GGGTGGTTGATCGCCTCC-3'; CYCB-F, 5'-TGCCCAGCGACTACATGAC-3', and CYCB-R, 5'-CGTCTCGGGCATCAGCTT-3' (Frej and Tulin, 2015).

Protein extraction

Chlamydomonas cells were harvested by centrifugation at 600 x *g* for 5 min*,* quick frozen in liquid nitrogen, and crushed with mortar and pestle. Protein extraction buffer [20 mM sodium phosphate buffer (pH 7.4) containing 100 μM Na_3VO_4, 50 mM β-glycerophosphate, 0.5 mM phenylmethanesulfonylfluoride (PMSF) and one tablet of Complete Protease Inhibitor Cocktail

(Roche)] was used to resuspend the cells (Fujita et al., 2013). After centrifugation at 15,000 x *g* for 20 min, the cell extracts were transferred to a new tube, added with 3 times volume of acetone, and incubated overnight at – 20°C. The protein extract was centrifuged at 15,000 x *g* for 10 min and resuspended in 1 x sample buffer (62.5 mM Tris-HCl, pH6.8, 2.5% SDS, 0.002% bromophenol, 10% glycerol). The protein concentration was measured using RC DC Protein Assay (Bio-rad) by using bovine serum albumin as a control. The absorbance readings were taken using Ultrospec 3000 UV/Visible spectrophotometer (Pharmacia Biotech) at 750 nm.

Immunoblotting

Proteins (20 μg) were resolved on 10% SDS-PAGE (Resolving gel: 375 mM Tris-HCl, 10% acrylamide, 0.1% SDS, 0.1% APS and 0.04% TEMED; stacking gel: 147 mM Tris-HCl, 5% acrylamide, 0.1% SDS, 0.1% APS and 0.1% TEMED) with a 1 x SDS running buffer (25 mM Tris, 192 mM glycine and 0.1% SDS). For phos-tag 10% SDS-PAGE, 50 mM MnCl and 25 μM Phos-tag (Wako) were added in addition of 10% SDS PAGE resolving gel mixture. The SDS PAGE electrophoresis were performed using voltage of 300 V, 40 mA for 100 min. After electrophoresis, the gel was washed in transfer buffer (25 mM Tris, 192 mM glycine and 10% methanol) for 5 min. Phos-tag gel was washed in transfer buffer with addition of 10 mM EDTA. The proteins were then blotted onto a polyvinylidene fluoride (PVDF) membrane (Immobilon-P, Merck Milipore) and electrophoresis was performed using transfer buffer for 60 min at 100V, 400 mA. After electrophoresis. the blotted membrane was washed with TBS-T buffer (20 mM Tris, 150 mM NaCl and 0.1% Tween 20) before blocked with blocking buffer (5% skim milk in TBS-T) for 1 hr. Then, the blotted membrane was incubated overnight with a primary antibody in the blocking buffer. Primary antibodies used in this study were anti-α-tubulin mouse antibody (B-5-1-2) (1:100,000 dilution) (Sigma) and anti-pT349 rabbit antibody (1:5,000 dilution) (Hotta et al., 2016). After washing with TBS-T three times, the membrane was incubated with anti-mouse IgG, HRP-linked antibody (GE-Healthcare; 1:10,000 dilution) or anti-rabbit IgG, HRP-linked antibody (GE-Healthcare; 1:10,000 dilution) as secondary antibodies in the blocking buffer for one hour. Immobilon western chemiluminescent HRP substrate (Milipore) was used for immunoblot detection. Chemiluminescence was detected using ImageQuant LAS4000 (GE Healthcare Life Sciences) and quantified by using Image J (Schneider et al., 2012).

Microscopy analyses

For immunofluorescence analysis, approximately 100 μL of *Chlamydomonas* cells were placed on a clean polylysine-coated microscopy slide, which had been prepared by treating the slide with 0.1 mg/mL of polylysine solution (Sigma-Aldrich) for 15 min. After immobilizing the cells on the polylysine slide for 5 min, 100 μL of PBS containing 4% (w/v) formaldehyde were applied to the cells for another 20 min. After washing with PBS three times, the slide was immersed in chilled methanol at – 20 °C for 20 min. The slide was washed with PBS three times again. Then, the slide was treated with 100 μL of blocking solution [5% (w/v) BSA in PBS-T buffer (PBS solution added with 0.1% of Tween 20)] for one hour, and then with primary antibodies. For double-labeling immunofluorescence experiments, anti-α-tubulin rat antibody (YOL 1/34) (Milipore) and anti-acetylated α-tubulin mouse antibody (B-6-1-1)(Sigma) were used. For α-tubulin single immunofluorescence experiment, anti-α-tubulin mouse antibody B-5-1-2 was used. All primary antibodies were applied at a dilution ratio of 1:2,000. The slide was incubated at 4°C overnight and then washed with PBS-T for three times. For double-label immunofluorescence experiments, goat anti-rat Alexa Fluor® 488 (Invitrogen) and goat anti-mouse Alexa Fluor® 568 (Invitrogen) were used. Donkey anti-mouse Alexa Fluor® 488 (Invitrogen) was used as a secondary antibody for the α-tubulin single immunofluorescence experiments. All secondary antibodies with a dilution ratio of 1:200 was added together with PBS-T to the slide and incubated for one hour. After washing with PBS-T three times, the slide was treated with a mounting solution (100 mM Tris, 50% glycerol and 1 mg/mL para-phenylenediamine) and covered with 22 x 22 mm coverslip. Microscopy slides were examined with a Nikon Eclipse T*i*-U microscope equipped with a Yokogawa CSU-XI spinning disc confocal unit and Nikon 100x/1.30 oil immersion objective lens. Images were captured and recorded at 0.5 μm intervals at the wavelength of 488 nm and 568 nm by using Andor iXon3 DU897 EM-CCD camera. All images were documented by stacking using Z series. Image J was used to merge images of two chromophores, and the brightness was adjusted. The occupancy of tubulin and acetylated tubulin were determined by using Image J. Binary image of *Chlamydomonas* cells created by image J was used to evaluate the occupancy of tubulin and acetylated tubulin in cell body over the cell size. The tubulin and acetylated tubulin occupancy values were subjected for statistical analysis. Statistical significance between the means of group was calculated by one-way ANOVA with Tukey HSD post-hoc test, where p-value <0.01 indicates significantly different.

To stain DNA, cells were fixed on a polylysine coated slide with 4% paraformaldehyde for 20 min. The slide was washed three times with PBS and incubated with PBS + 500 nM Sytox green (Invitrogen) for 30 min (modified from Tulin & Cross, 2014). Mounting medium was applied and cover slides placed.

For bright field microscopy, cells were treated with 1% glutaraldehyde and placed onto a microscope slide. Microscope slides were examined by using Nikon Eclipse E600 fluorescence microscope (Nikon) with Nikon 40x/0.75 objective lens. All mages were captured using Olympus DP70 camera and documented using DP controller software (Olympus).

RESULTS

PHS1 genes in algae

I searched the publicly available genome databases of red algae (Rhodophyta) and green algae (Chlorophyta). Since the tubulin kinase domain possessing an atypical kinase domain with high homology to the unique actin-fragmin kinase domain (Steinbacher et al., 1999) is a hallmark of the evolution of PHS1, I first searched the presence of the tubulin kinase-like sequences. Kinase domains with high sequence similarity to the tubulin kinase domain were not found in the genomes of red algae. However, tubulin kinase domains were identified in many (but not all) genomes of green algae (Table 1). Every algae protein possessing the tubulin kinase had an MAP kinase phosphatase-like domain in its C-terminus. Therefore, these proteins share the overall domain architecture of PHS1.

In Chlorophyta, *PHS1* genes are present in nine Chlorophyceae species (*Chlamydomonas reinhardtii*, *Chlamydomonas eustigma*, *Chlamydomonas incerta*, *Chlamydomonas schloesseri*, *Chromochloris zofingiensis*, *Edaphochlamys debaryana*, *Gonium pectoral*, *Monoraphidium neglectum*, and *Scenedesmus* sp. NREL), five Trebouxiophyceae species (*Picochlorum soloecismus*, *Auxenochlorella protothecoides*, *Chlorella variabilis*, *Coccomyxa subellipsoidea*, and *Micractinium conductrix*), and one Maiellophyceae species (*Micromonas pusilla*). These green algae live in freshwater except for *P. soloecismus* (brackish water) and *M. pusilla* (marine). The tubulin kinase domain in the predicted PHS1 protein in the marine-living *M. pusilla* has somewhat lower sequence homology (38%; also see the phylogenetic tree of the PHS1 kinase domain in Figure 7) and contains two unique insertions of 17 and 41 amino acid residues that are not found in other algal PHS1 sequences (Figure 8). It is noteworthy that two marine green algae, *Bathycoccus prasinos* (Maiellophyceae) and *Dunaliella salina* (Chlorophyceae), do not possess any *PHS1*-like genes in their genomes. Possible correlation between the presence of PHS1 and the non-saline habitat is discussed later.

Tubulin is phosphorylated under salt and osmotic stress in *Chlamydomonas*

As a representative model green algae, I focused on *Chlamydomonas reinhardtii*. Various laboratory strains were examined for stress-induced tubulin phosphorylation. The C9 and C125 strains possess normal cell wall, whereas the C5155, C5325 and CC4533 strains have defects in

cell wall components (Chlamydomonas Resource Center; https://www.chlamycollection.org/). These strains were treated either with NaCl at 0.1 M, 0.2 M, and 0.5 M, or with sorbitol at 0.1 M, 0.2 M, and 0.6 M for 20 min, and then analyzed for α-tubulin phosphorylated at Thr349 by a specific phosphor-tubulin antibody. This antibody was raised against a phospho-peptide (N-FVDWCPpTGFKCGIN-C) targeting the *Arabidopsis* α-tubulin Thr349 (Hotta et al., 2016). This peptide sequence is perfectly conserved in the two α-tubulins of *C. reinhardtii*. The immunoblot results in Figure 9 showed that all strains, regardless of intact or defective cell walls, phosphorylated α-tubulin at Thr349 upon treatment with 0.1- 0.2 M NaCl and with 0.2 M sorbitol. Phosphorylation of α-tubulin at Thr349 was also detected in the non-targeted phosphor-proteome analysis of *C. reinhardtii* proteins (Werth et al., 2017). At higher concentrations of sorbitol (0.6 M) and salt (0.5 M), tubulin phosphorylation was not detected. *Chlamydomonas* cells did not grow under these stress conditions, indicating that severe stresses halt cell metabolisms and stress signaling pathways that lead to activation of PHS1.

Since the CC-4533 strain possesses a *cw15* wall-deficient mutation (Monk et al., 1983), which enables a facile genetic transformation (Shimogawara et al., 1998), and is used for the Chlamydomonas Library Project (Li et al., 2019), I used this strain for all the subsequent analyses. To further investigate stress response under the saline environment, commercial artificial seawater composed of sodium chloride, sodium, calcium chloride, magnesium chloride and other minor minerals was applied for 10 min at the concentrations of 10%, 20%, 40% and 60%, which is equivalent of approximately 0.05 M, 0.1 M, 0.2 M and 0.3 M NaCl (Figure 10). Tubulin phosphorylation was detected at 20% and 40% of seawater but not at 10% and 60%. Salt concentration may be a major factor that triggers tubulin phosphorylation.

PHS1 mediates stress-induced tubulin phosphorylation

The single-copy *PHS1* gene (Cre08.g375000) is located at chromosome 8 of *Chlamydomonas reinhardtii*, consists of 17 exons and 16 introns, and potentially encodes a polypeptide of 1,905 amino acid residues (Figure 11). The positions of introns were supported by an RNAseq analysis (H. Fukuzawa, personal communication). The predicted *Chlamydomonas* PHS1 protein is much longer than PHS1 proteins from other plants, such as *Arabidopsis thaliana* PHS1 of 929 amino acid residues (Data not shown). The sequence expansion of *Chlamydomonas* PHS1 occurs in the region between the tubulin kinase domain and the phosphatase domain, and is highly abundant in

Gly and Ala. Other *Chlamydomonas* species, such as *C. incerta*, and *C. shloesseri* also has similar Gly- and Ala-rich insertions at the same position, but their amino acid sequences of the insertions are somewhat variable (Data not shown). Apparently, these *Chlamydomonas*-specific inter-domain insertions do not abrogate catalytic and regulatory functions of the algal PHS1s.

To examine whether *Chlamydomonas* PHS1 is responsible for the observed tubulin phosphorylation, three independent T-DNA insertion lines at the *PHS1* locus were obtained (Figure 11). No tubulin phosphorylation was detected upon salt stress in these *phs1-1*, *phs1-2* and *phs1-3* alleles (Figure 12), indicating that these mutants are loss-of-function alleles. Since the *phs1-1* cells grew slowly even in the absence of stress and since the *phs1-3* cells showed unreproducible growth responses over the repeated experiments during one year, I mostly analyzed the *phs1-2* allele. A PHS1 genomic fragment of 11 kb, comprising of a 399 bp 5'-upstream sequence and a 2046 bp-3'-sequence, was transformed to the *phs1-2* allele. Genomic PCR amplification using the primer set targeting a region flanking the T-DNA insertion site in the 12th intron (P1 and P2) and using the primer set that would amplify the junction between the 12th exon and the T-DNA left border (P1 and LB) confirmed that PHS1 was disrupted by T-DNA in *phs1-2* and its complementation line, whereas an intact PHS1 region of 1.2 kb was present in the genomes of both wild type and the complementation line (Figure 13). Treatment of 0.2 M sorbitol for 10 min induced tubulin phosphorylation in wild type and the complementation line, but not in *phs1-2*, indicating recovery of a tubulin kinase activity by the introduction of the wild-type *PHS1* copy in the *PHS1* null mutant (Figure 14).

Establishment of synchronized *Chlamydomonas* cell cultures

In order to analyze cell growth and cell biological phenotypes separately in interphase and mitosis, growth of *Chlamydomonas* cells was synchronized by adjusting an inoculum at the beginning of the culture and by alternating the illumination in a 12 hour light-12 hour dark cycle. Several criteria were used to evaluate the degree of synchronization. Expression patterns of two cell-cycle regulated genes were analyzed by reverse transcription qPCR. *CDKB* and *CYCB* are a cyclin-dependent kinase gene and a cyclin gene, respectively, which are specifically up-regulated during the S/M phase of the *Chlamydomonas* cell cycle (Bisova et al., 2005; Tulin and Cross, 2015). The expression levels of these two genes were low at the beginning of the synchronized culture, increased sharply at the 10th hour before the start of the dark period, and then started to decrease

after 12th hour (Figure 15). Next, I used a coulter counter and a light microscopy to analyze the number, the size and the morphology. The *Chlamydomonas* cell size showed Gaussian distribution patterns, and the size distribution peaks increased while maintaining the initial cell number until the 12th hour, when the cells increased the cell volume approximately eight fold (Figure 16). After the onset of the dark period at the 12th hour, the number of free daughter cells began to increase and, by the 16th hour, the cell number increase stopped and all the cells were small as the beginning of the culture. Microscopic images of individual cells at each cell cycle stage supported the coulter counter analyses, and further showed that *Chlamydomonas* cells formed daughter cell aggregates (palmelloids) that peaked at the 12th to 13th hour (Figure 16). Individual daughter cells in a palmelloid were released (i.e., the palmelloid was hatched) after the 14th hour. The cell number analysis by the coulter counter does not differentiate palmelloids from free single cells (Figure 17). Altogether, these analyses show that I attained a high level of cell cycle synchronization and that under my synchronization conditions the cells are in the interphase from the start of the culture to the 10th hour, while the mitosis occurs between the 10th and the 13th hour.

In the subsequent studies, I analyzed the phenotypes using the synchronized cells.

Effects of salt and sorbitol on tubulin phosphorylation and cell growth

Both sorbitol and salt induce hyperosmotic stress to the cells, while the effects of high concentrations of salt also involve cellular ion imbalance (Verslues et al., 2006). When the effects of sorbitol and NaCl were compared at the similar osmolarity, comparable levels of the tubulin phosphorylation were observed. For example, 0.3 M sorbitol and 0.15 M NaCl give comparable levels of osmotic pressure. When *Chlamydomonas* cells were treated by 0.3 M sorbitol or 0.15 M NaCl, tubulins were phosphorylation at similar levels after 10 min (Figure 18, Table 2). These concentrations of sorbitol and NaCl, however, affected the cell growth differently; NaCl at 0.15 M inhibited the cell volume increase much more severely than sorbitol at 0.3 M (Figure 19). These results suggest that the tubulin phosphorylation is mainly caused by hyperosmotic stress and that the inhibition of cell growth by salt involves effects other than the osmotic stress. Therefore, I will hereafter mainly use sorbitol to apply hyperosmotic stress to the cells.

Sorbitol triggers rapid and transient tubulin phosphorylation

Effects of sorbitol were studied in interphase (at the 6th hr) and mitosis (at the 11th hr). In the interphase cells, sorbitol at 0.2 M and 0.3 M induced high tubulin phosphorylation at 10 min of stress treatment; thereafter, tubulins were swiftly dephosphorylated by 1 hr (Figure 20). In the mitotic cells, similar patterns of tubulin phosphorylation and dephosphorylaiton were observed, but there were low levels of phosphorylated tubulins detected even in the absence of the stress, and tubulin dephosphorylation took somewhat longer time to complete.

To determine how much tubulins are phosphorylated, I next used a phosphor-protein-interacting chemical, the phos-tag (Kinoshita et al., 2006) to separate phosphorylated and non-phosphorylated proteins by phos-tag SDS PAGE (Figure 21). The peaks of tubulin phosphorylation occurred after 10 min (interphase) and 30 min (mitosis) of 0.3 M sorbitol treatment, and more than 60% of cellular tubulins were phosphorylated at the peaks (Table 3). Lower levels of tubulin phosphorylation in the interphase cells may reflect that the flagellar microtubules are highly stable and only exchange with cellular tubulins at the flagellar tips (Orbach and Howard, 2019; van de Weghe et al., 2020).

These results demonstrate that hyperosmotic stress induces rapid, massive, and transient tubulin phosphorylation in both interphase and mitotic cells of *C. reinhardtii*.

Microtubules are transiently disassembled by PHS1 in sorbitol-treated cells

To examine the consequences of stress-induced transient tubulin phosphorylation on microtubule organization, microtubules were labeled by both anti-α-tubulin antibody and anti-acetylated-α-tubulin antibody. Acetylated tubulins are specifically present in stable and long-lived microtubules and protect microtubules from mechanical breakage (Xu et al., 2017). In interphase *Chlamydomonas* cells, four microtubule bundles, called “rootlets” extend from the basal body toward the other end of the cell body along the cell periphery, and are known to contain acetylated tubulins, indicating their partial stability (LeDizet and Piperno, 1986). In the non-stressed control cells, a few thick microtubule bundles that often contain some acetylated tubulins were discernible and most likely represent microtubule rootlets (Figure 22). Flagellar microtubules are substantially acetylated (Piperno and Fuller, 1985), and were also strongly stained in my study. Microtubule organizations were indistinguishable among wild type, *phs1-2*, and its complementation line. Upon sorbitol treatment for 10 min, interphase microtubules in wild type and the complementation line

were considerably depolymerized, whereas such rapid microtubule disassembly did not occur in *phs1-2*. Levels of acetylated tubulins increased in the mutant cells, indicating that hyperosmotic stress transiently stabilized microtubules, although it is not clear whether this apparent PHS1-independent microtubule stabilization and the PHS1-mediated microtubule destabilization (by tubulin phosphorylation) functionally antagonize in wild-type cells. After 1 hr of stress treatment, microtubule organization in wild type and the complementation line recovered to the initial non-stress levels. These results indicate that the PHS1-mediated tubulin phosphorylation leads to transient microtubule instability in interphase cells. Such stress-trigged microtubule reorganization is effective only for a short time window of less than 1 hr. Quantification and statistical analysis of the microtubule polymer density in cells confirm these results (Figure 23 and 24).

Cell growth is not affected by PHS1-mediated microtubule destabilization

The above results show that hyperosmotic stress depolymerizes interphase microtubules for a short period (less than one hour). I first examined whether such a transient microtubule destabilization affects cell growth during interphase. In *Chlamydomonas* cells in which cell growth and cell division are partially uncoupled, how fast cells grow during a prolonged G1 phase determines how many multiple fission cycles occur after the light period (Umen, 2018). Hyperosmotic stress was applied at the onset of synchronization culture by inoculating *Chlamydomonas* cells into culture media containing 0.2 M or 0.3 M sorbitol. Increase in the cell volume was monitored during growth in the sorbitol-containing media (Figure 25). There were apparently not differences in the growth rates of wild type, *phs1-2*, and the complementation line. Growth rates from repeated experiments were calculated for the initial log phase (up to 3 hours after inoculation) and for the later accelerated growth phase (from 6 to 9 hours). Increasing concentrations of sorbitol inhibited cell growth more strongly during the accelerated growth phase, but the growth rates for both phases were indistinguishable among the three genotypes. These results show that PHS1 does not play any obvious roles in cell growth during interphase.

Next, dividing cells were targeted for osmotic stress, by applying sorbitol just before the onset of mitosis (at the 9th hour). The *Chlamydomonas* cell cycle progression was delayed after sorbitol treatment (Figure 26). There is no statistically differences of cell volume between wild-type, *phs1-2* and complementation line during the stress treatment. However, more palmelloids (~18%) were observed in *phs1-2* compared to wild type and the complementation line (Figure 26). Bright field

microscopic images showed that several palmelloids were observed in *phs1-2* cells after 3 hours of stress application (the 12th hour after the onset of culture), but not in wild-type and the complimented cells (Figure 26c). Therefore, I conclude that the delayed cell cycle progression after stress was partly caused by the PHS1 functions.

Effects of drug-induced microtubule destabilization on cell growth and cell division: a comparative study

PHS1-mediated microtubule destabilization may not cause apparent effects on cell growth and cell division because of its transient nature. I therefore asked whether persistent microtubule destabilization affect cell cycle progression in *Chlamydomonas* cells. A benzamide-type tubulin-binding drug, propyzamide, is reported to effectively depolymerize microtubules of the algae cells (Schibler and Huang, 1991), and thus was used in my study. Wild-type *Chlamydomonas* cells were grown in the culture media containing propyzamide at 3, 5, or 10 μM (Figure 27). In the presence of propyzamide at 10 μM, microtubules were effectively depolymerized at the 6th hour and the 24th hour of culture (Figure 28). Propyzamide did not affect the cell growth at interphase but caused a delay in the progression of mitosis in a dose-dependent manner up to 5 μM. At 10 μM, the treated cell did not divide and became a large cell containing a single large nucleus, which was stained by the Sytox green dye (Figure 29).

These results demonstrate that microtubules have not essential roles in interphase cell growth, which is consistent with our inability to detect any growth phenotypes in the sorbitol-treated *phs1* mutant cells. Cell cycle progression was delayed and even halted by increasing destabilizing mitotic microtubules. If I were to observe any cell division effects by PHS1, the time course of cell division need to be carefully analyzed in the presence of timely hyperosmotic stress.

Organism (Protein ID)	Class	Presence in the genome		Habitat
		Tubulin kinase (Similarity*)	Juxtaposed phosphatase	
Bathycoccus prasinos (NCBI: XP_007513221.1)	Mamiellophyceae	No	---	Marine
Micromonas pusilla (PhycoCosm: wlab.224067.1)	Mamiellophyceae	Yes? (38%)	Yes	Marine
Dunaliella salina (NCBI: KAF5837797)	Chlorophyceae	No	---	Marine
Picochlorum soloecismus (PhycoCosm: NSC_00507-R1)	Trebouxiophyceae	Yes (49%)	Yes	Brackish water
Auxenochlorella protothecoides (NCBI: XP_011399729.1)	Trebouxiophyceae	Yes (45%)	Yes	Freshwater
Chlorella variabilis (NCBI: XP_005847636.1)	Trebouxiophyceae	Yes (52%)	Yes	Freshwater
Coccomyxa subellipsoidea C-169 (PhycoCosm: estExt_fgenesh1_pg.C_140051)	Trebouxiophyceae	Yes (47%)	Yes	Freshwater
Micractinium conductrix (UniProt: A0A2P6VK31)	Trebouxiophyceae	Yes (53%)	Yes	Freshwater
Chlamydomonas eustigma (PhycoCosm: rna-CEUSTIGMA_g1784.t1)	Chlorophyceae	Yes (48%)	Yes	Acidic water
Chlamydomonas reinhardtii (UniProt: A0A2K3DHM7)	Chlorophyceae	Yes (50%)	Yes	Freshwater
Chlamydomonas incerta SAG 7.73 (PhycoCosm: g13682.t1)	Chlorophyceae	Yes (48%)	Yes	Freshwater
Chlamydomonas schloesseri CCAP 11/173 (PhycoCosm: g14248.t1)	Chlorophyceae	Yes (48%)	Yes	Freshwater
Chromochloris zofingiensis (PhycoCosm: Cz19g00060.t1)	Chlorophyceae	Yes (50%)	Yes	Freshwater
Edaphochlamys debaryana CCAP 11/70 (PhycoCosm: g9287.t3)	Chlorophyceae	Yes (48%)	Yes	Freshwater
Gonium pectoral (UniProt: A0A150H3H5)	Chlorophyceae	Yes (46%)	Yes	Freshwater
Monoraphidium neglectum (NCBI: XP_013906388.1)	Chlorophyceae	Yes (43%)	Yes	Freshwater
Scenedesmus sp. NREL (PhycoCosm: CE926008_1917)	Chlorophyceae	Yes (52%)	Yes	Freshwater

Table 1. PHS1 in Chlorophyta green algae. PHS1 was identified by a high homology to the tubulin kinase domain and a juxtaposed MAP kinase phosphatase-like phosphatase. **Arabidopsis thaliana* PHS1 protein was used as a query sequence.

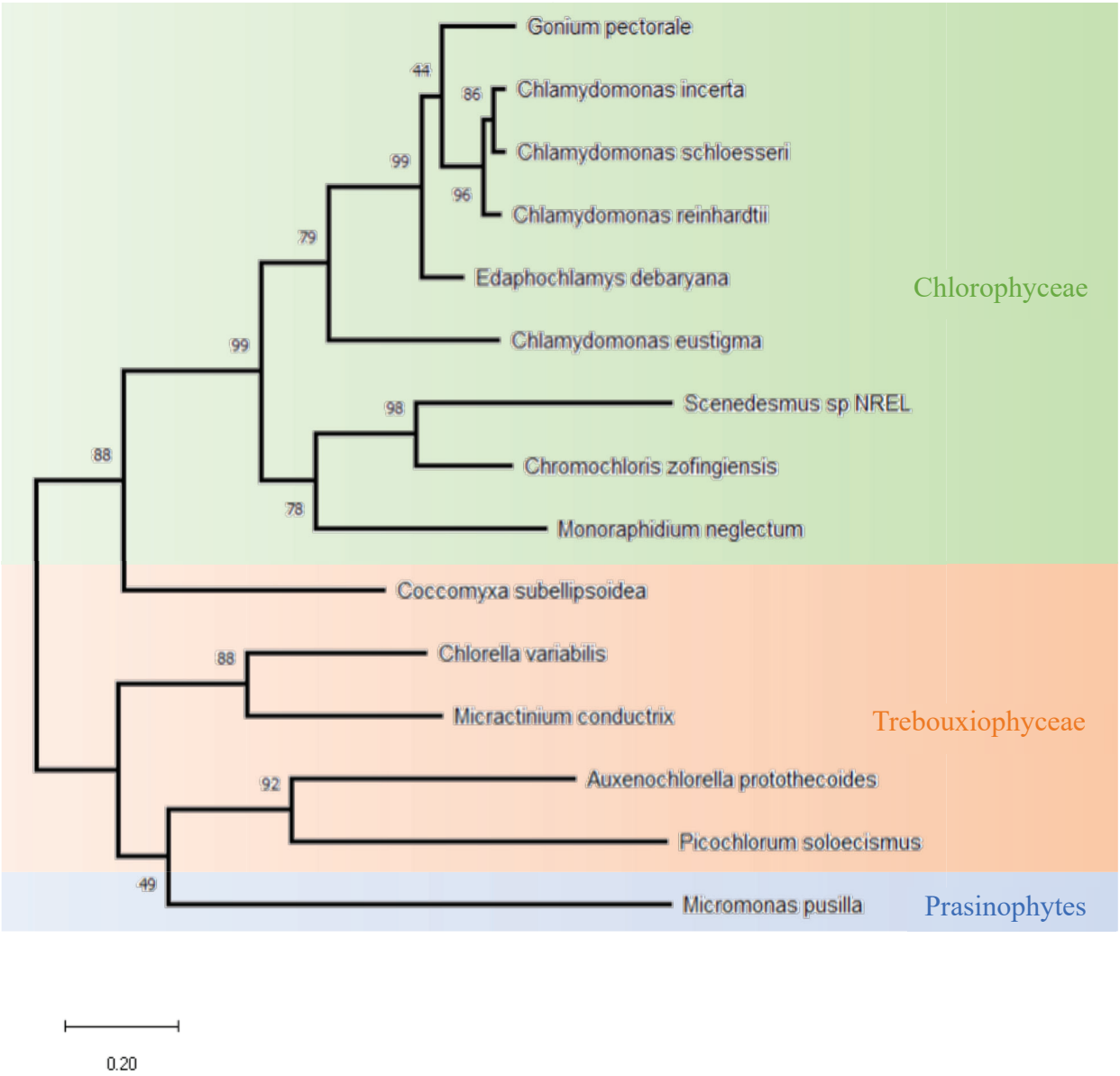

Figure 7: Phylogenetic tree of tubulin kinase domains in Chlorophyta green algae. Bootstrap values are indicated at each phylogeny lineage.

Figure 8: Alignment of tubulin kinase domains in the putative Chlorophyta PHS1s. In the *Microsomas pussila* PHS1, two insertions are found.

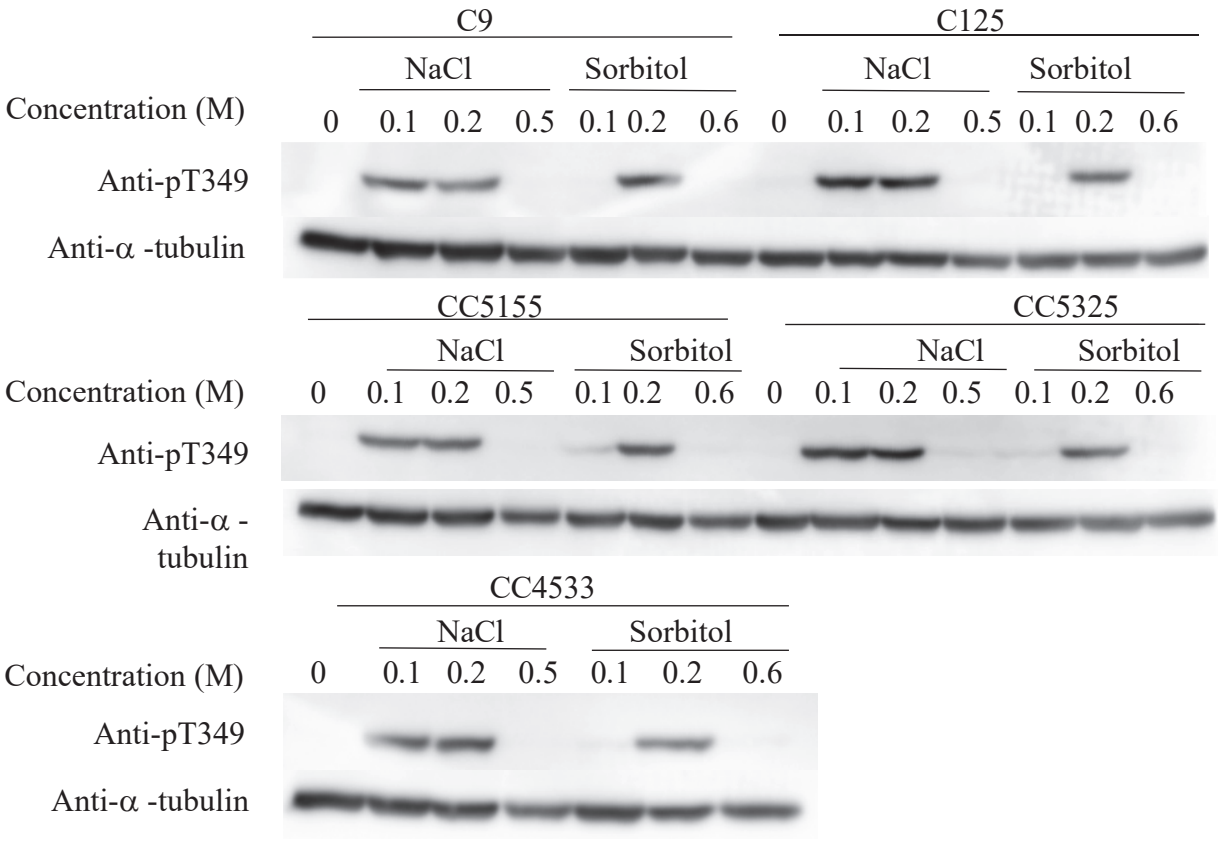

Figure 9: Immunoblot of cell-wall (C9, C125) and cell wall-deficient (CC5155, CC5325 and CC4533) *Chlamydomonas* strains treated by NaCl or sorbitol at the indicated concentration for 20 min. Proteins were separated by SDS-PAGE, blotted on membranes, and analyzed by anti-pT349 antibody or anti-α-tubulin antibody.

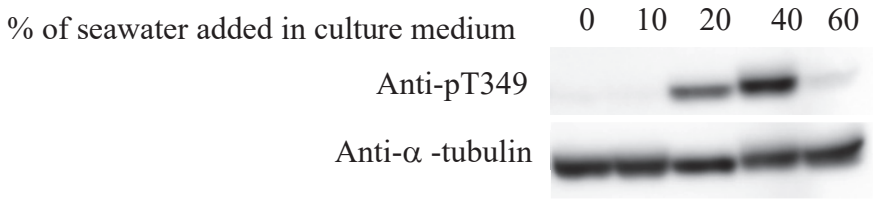

Figure 10: Immunoblot of *Chlamydomonas* cells (CC4533) treated by 0 – 60% of seawater for 10 min. Other conditions are the same as shown in Fig. 9.

Figure 11: Gene structure of PHS1. The boxes and connecting lines indicate exons and introns, respectively. Insertions of all T-DNA mutants (*phs1-1*, *phs1-2* and *phs1-3*) are shown in the *PHS1* gene. The tubulin kinase and phosphatase domains are shown in blue and red boxes, respectively. Blue arrows indicate primers used in genomic PCR.

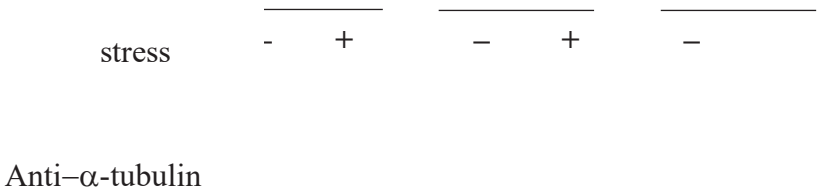

Figure 12: I *1-2*, and *phs1-3* cells treated with 0 or 0.1 M NaCl for 20 min. Other conditions are the same as shown in Fig. 9.

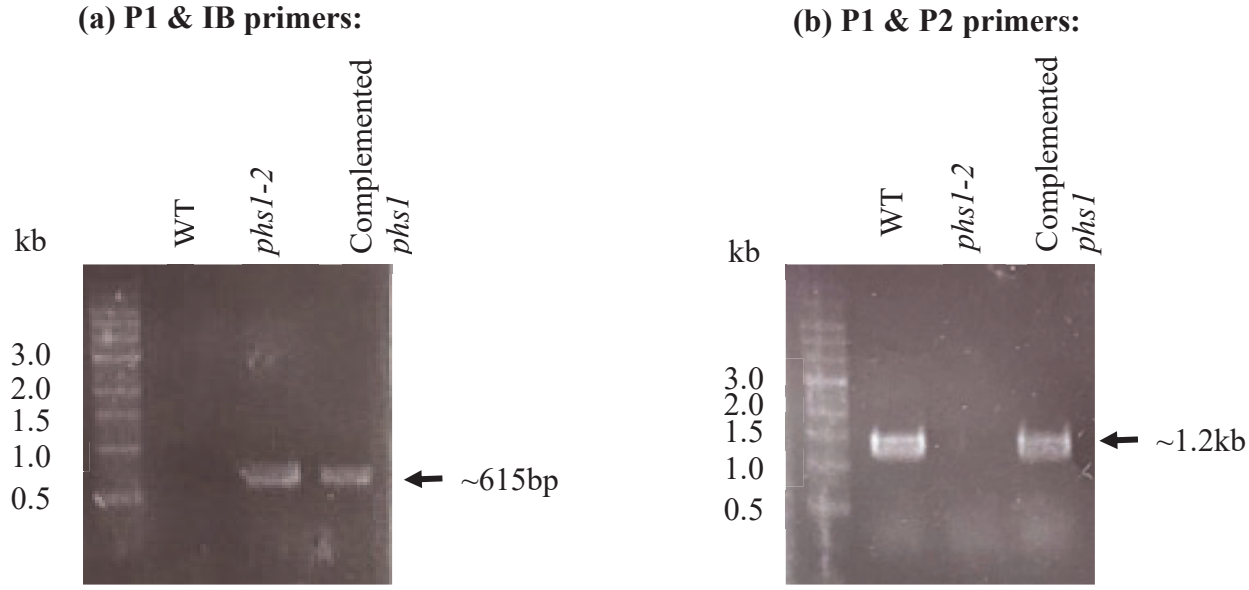

Figure 13: Agarose gel of *Chlamydomonas*, *phs1-2* and complemented *phs1-2* using primers targeting (a) on the *phs1* gene and T-DNA insertion cassette and (b) T-DNA insertion sites of *phs1-2.* PCR was performed using genomic DNA of wild type (WT), *phs1-2* and complemented *phs1*.

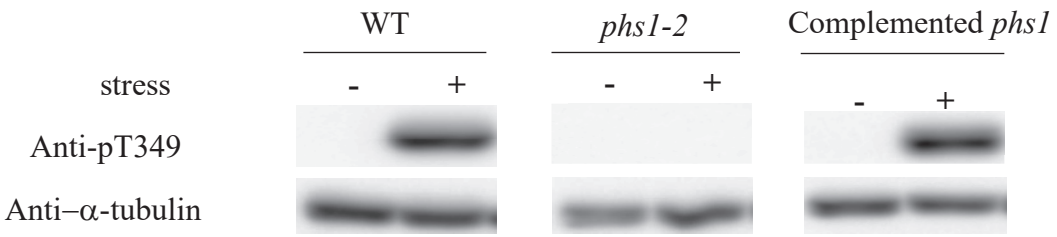

Figure 14: Immunoblot of *Chlamydomonas* WT, *phs1-2* and complemented line treated with 0 or 0.2 M sorbitol for 10 min. Other conditions are the same as shown in Fig. 9.

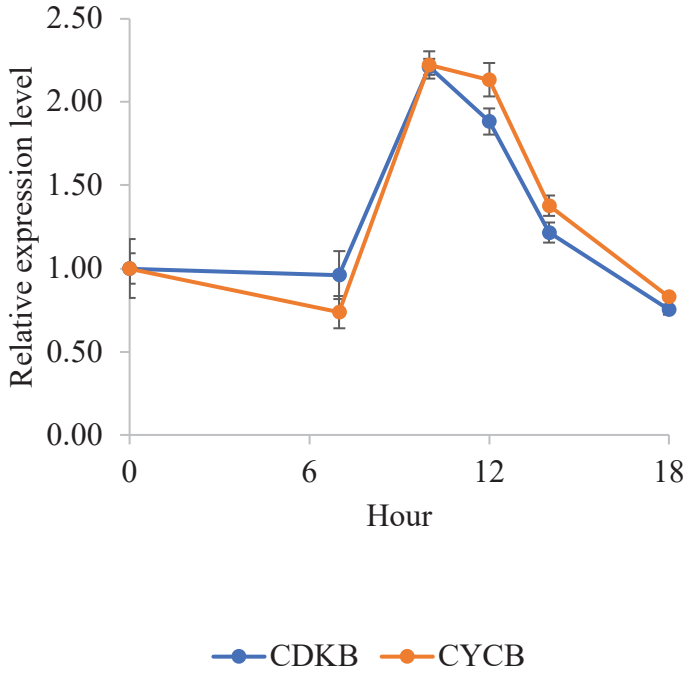

Figure 15: The expression level of *CDKB* and *CYCB* genes in *Chlamydomonas* cells. *Chlamydomonas* cells were cultured in a 12/12 hr light/dark diurnal cycle. Transcript levels were measured by qRT-PCR, and are shown relative to the levels of *PTB-1* gene. Error bars indicate standard deviation for three biological replicates.

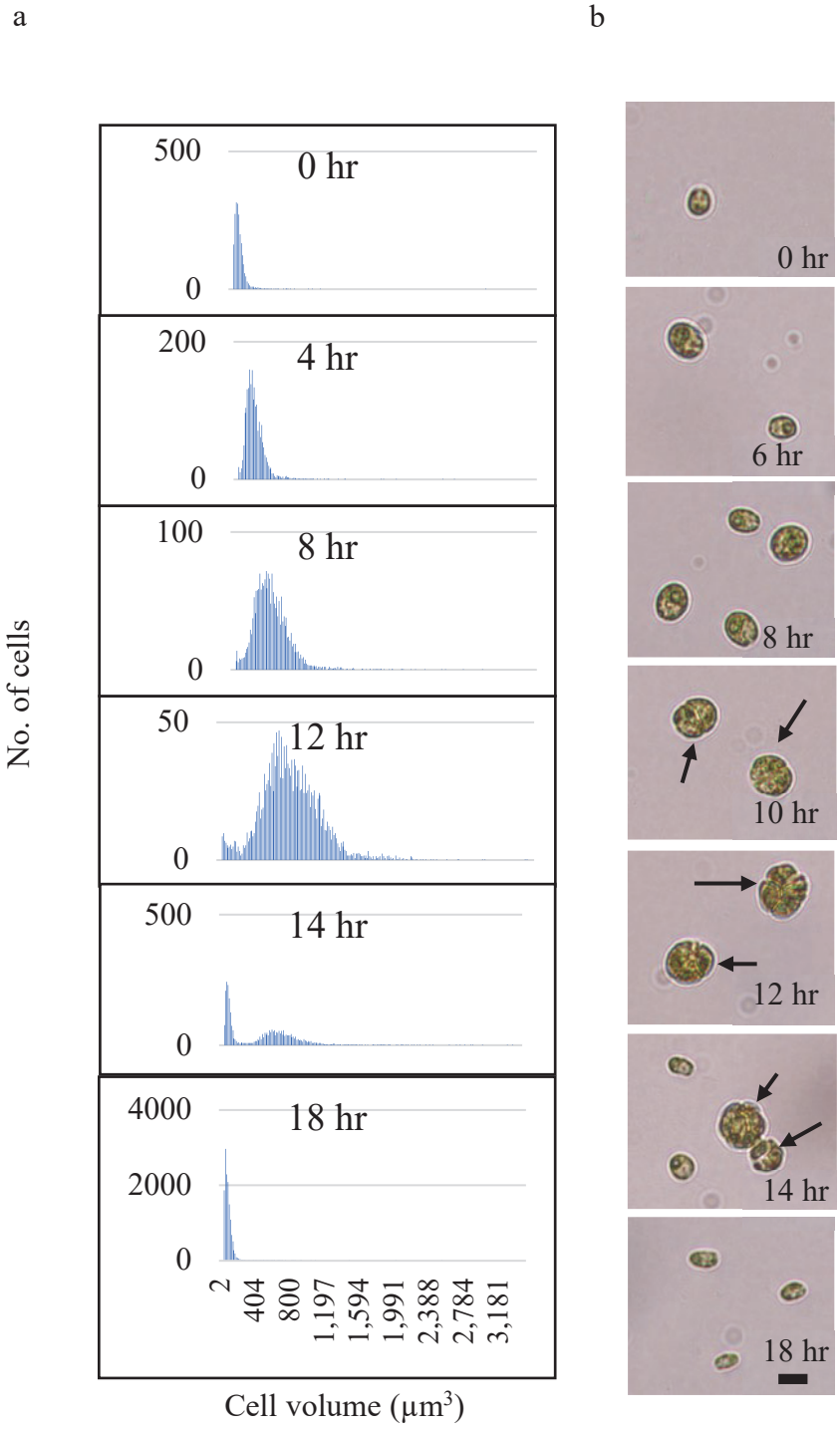

Figure 16: Cell size distribution of *Chlamydomonas* in a 12/12h of light/dark diurnal cycle. (a) Histogram showed *Chlamydomonas* cell size distribution at 0, 4, 8, 12, 14 and 18 hr in cell volume (μm^3) measurement, (b) bright field microscopic images of *Chlamydomonas* cells at 0, 6, 8, 10, 12, 14 and 18 hr. Arrows indicate of *Chlamydomonas* palmelloid. Bar indicates 10 µm.

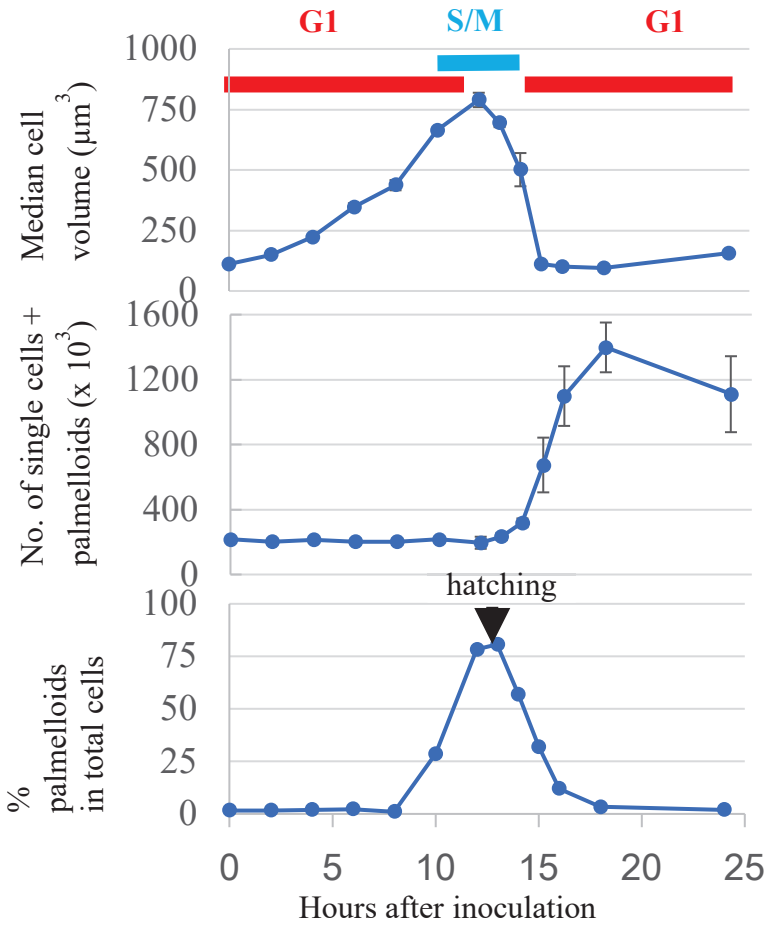

Figure 17: Synchronized *Chlamydomonas* cell culture. (a) median cell volume, (b) total number of cells, including single cells and palmelloids, and (c) percentage of palmelloids in total cells. Cells were cultured in a 12 hr/12hr light/dark diurnal cycle. The red and blue color boxes indicate the G1 and S/M phase, respectively. Error bars indicate standard deviation for three biological replicates.

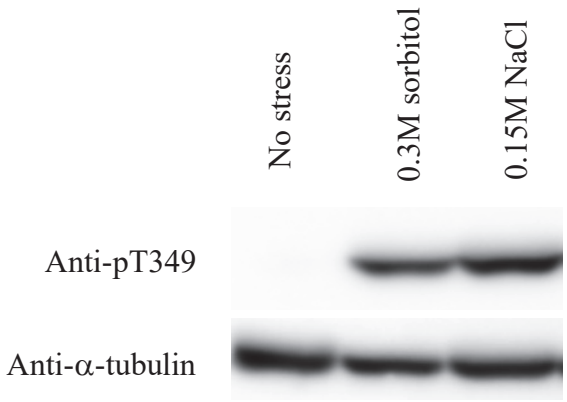

Figure 18: Immunoblot of *Chlamydomonas* cells treated with 0, 0.3 M sorbitol and 0.15 M NaCl for 10 min. Sorbitol and NaCl at the same osmolarity induce comparable levels of tubulin phosphorylation. Other conditions are the same as shown in Fig. 9.

Stress treatment condition	Relative phosphorylated tubulin intensity
0.3 M sorbitol	1.00
0.15 M NaCl	1.16

Table 2: Relative phosphorylated tubulin intensity of 0.3 M sorbitol and 0.15 M NaCl in Figure 18.

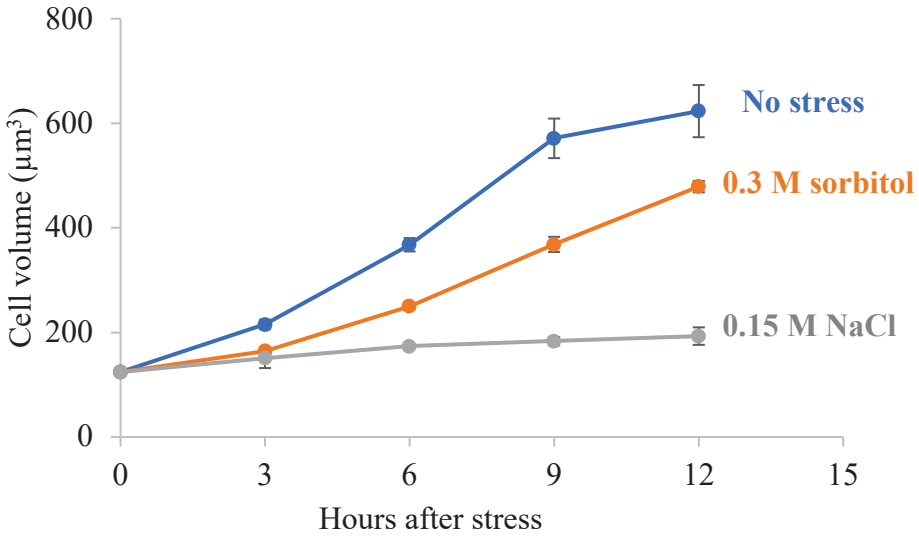

Figure 19: Cell volume of *Chlamydomonas* cells treated with 0, 0.3 M sorbitol and 0.15 M NaCl for 12 hours. Error bars indicate standard deviation for three biological replicates.

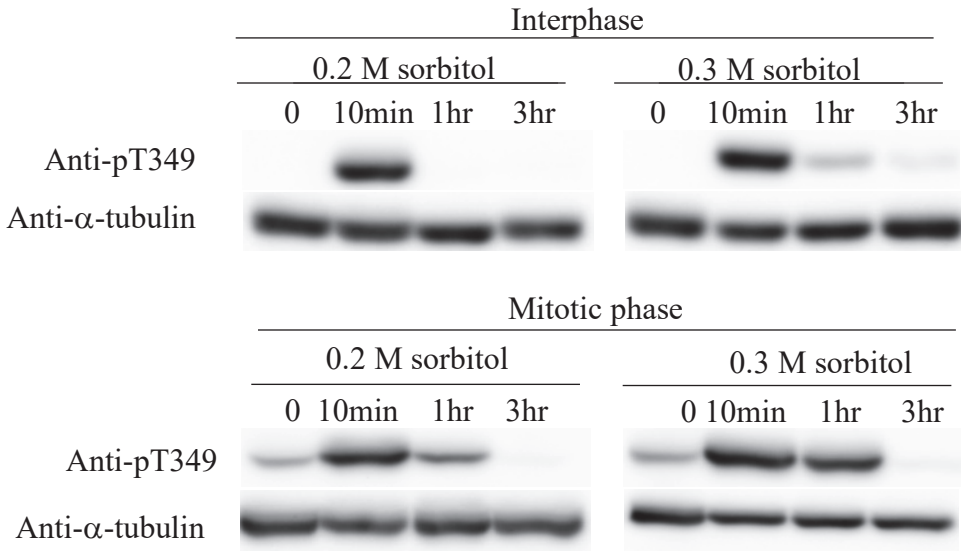

Figure 20: Immunoblot of phosphorylated tubulins in interphase and mitotic *Chlamydomonas* cells treated with 0.2 M and 0.3 M sorbitol for 0, 10 min, 1 hour and 3 hours. Sorbitol treatments were applied 6 hr after the start of light period (interphase cells) and 11 hr after the start of light period (mitotic cells). Other conditions are the same as shown in Fig. 9.

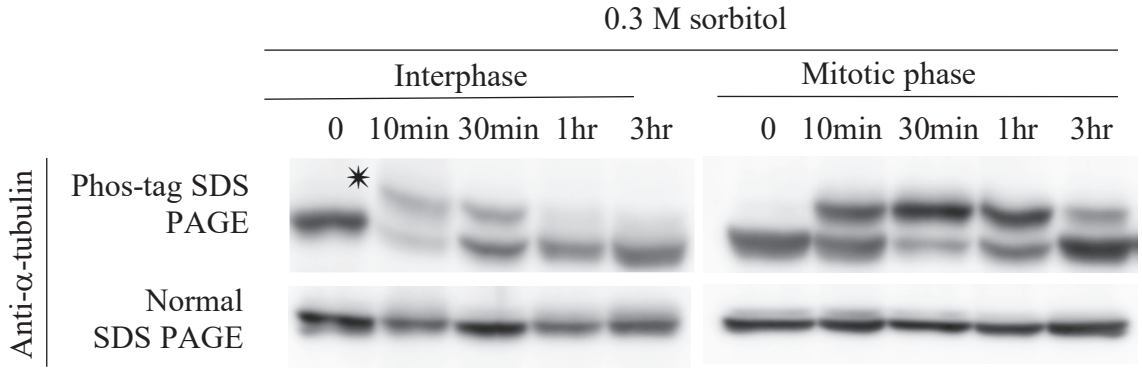

Figure 21: Immunoblot of tubulins in *Chlamydomonas* cells, using phos-tag and normal SDS PAGE gels. Upper bands in the phos-tag gels are phosphorylated forms. Stress treatment was applied 6 hr after the start of light period (interphase cells) and 11 hr after the start of light period (mitotic cells). Other conditions are the same as shown in Fig. 9.

	Interphase					Mitotic phase				
Time	0	10 min	30 min	1 hr	3 hr	0	10 min	30 min	1 hr	3 hr
Phosphorylated tubulin	0.04	0.60	0.35	0.16	0.17	0.03	0.45	0.74	0.59	0.42
Non-phosphorylated tubulin	0.96	0.40	0.65	0.84	0.83	0.97	0.55	0.26	0.41	0.58

Table 3: The relative phosphorylated and non-phosphorylated tubulin intensities in the phos-tag SDS PAGE gels in Figure 19.

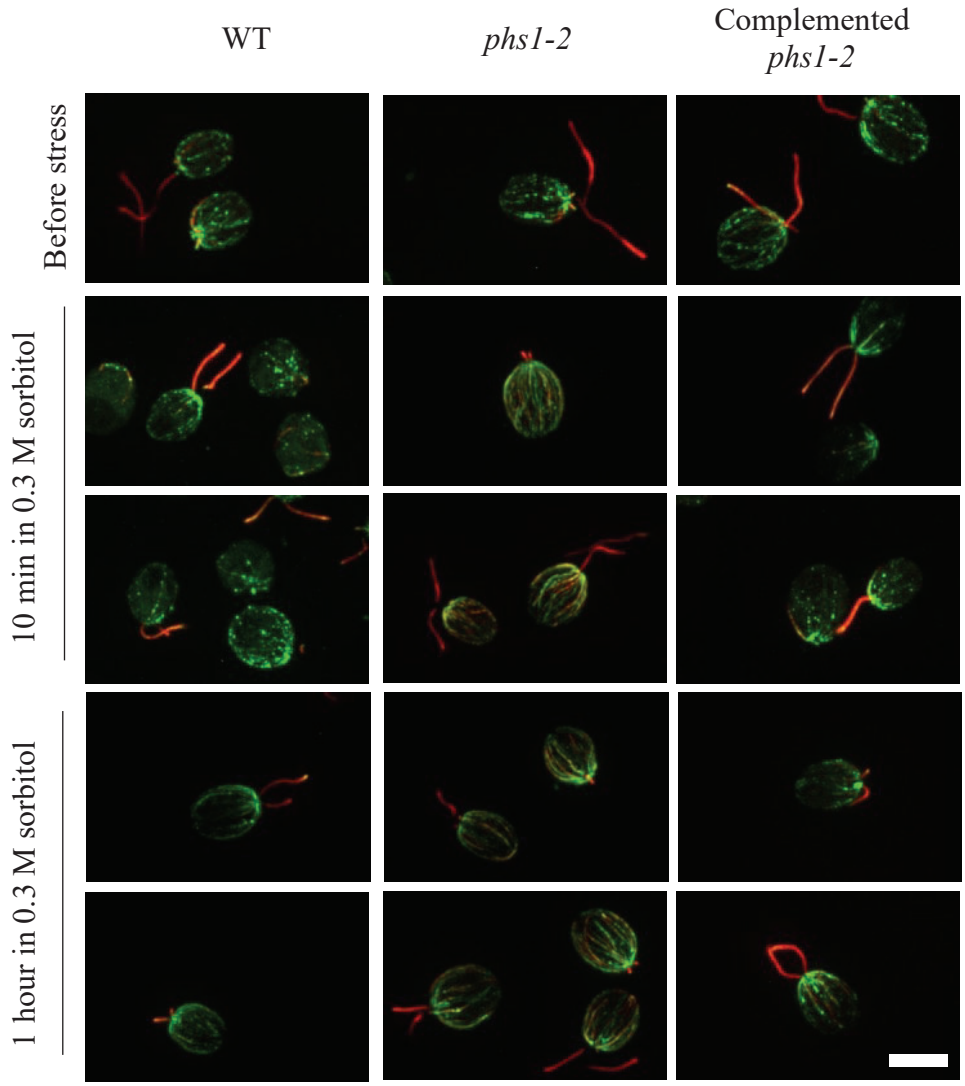

Figure 22: Combined immunofluorescence microscopic images of *Chlamydomonas* cells in 0.3 M sorbitol for 10 min and 1 hr. Stress treatment was applied at 6 hr after the start of light period. Cells were labeled with anti-acetylated tubulin (red) and anti-α-tubulin (green) antibodies. Bar indicates 10 μm.

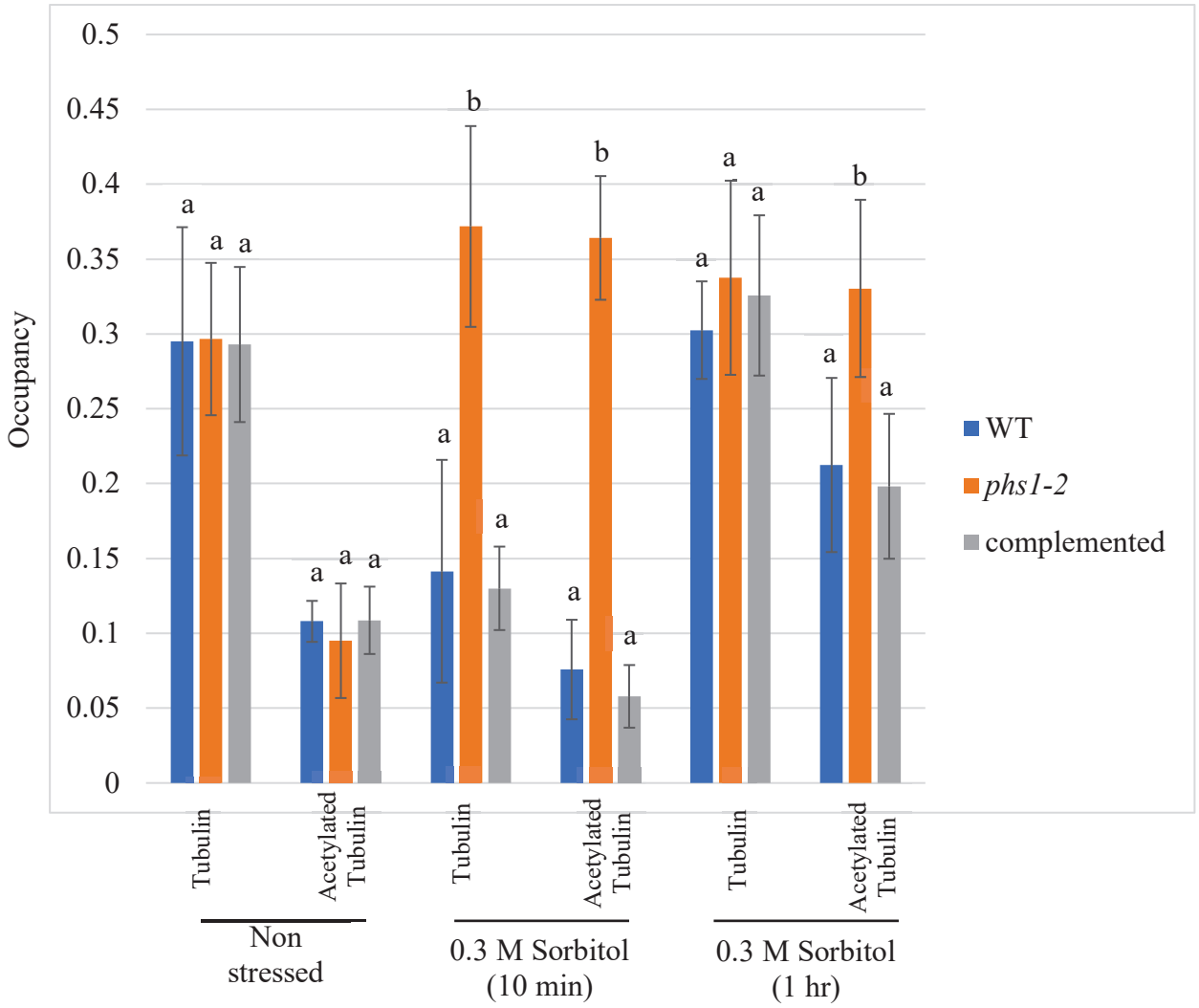

Figure 23: Occupancy of tubulin and acetylated tubulins in *Chlamydomonas* cells (n = 10) under 0 and 0.3 M sorbitol for 10 min and 1 h. Statistical significance between mean values was calculated by using one-way ANOVA with Tukey-HSD post-hoc test, where p-value <0.01 indicates significant difference.

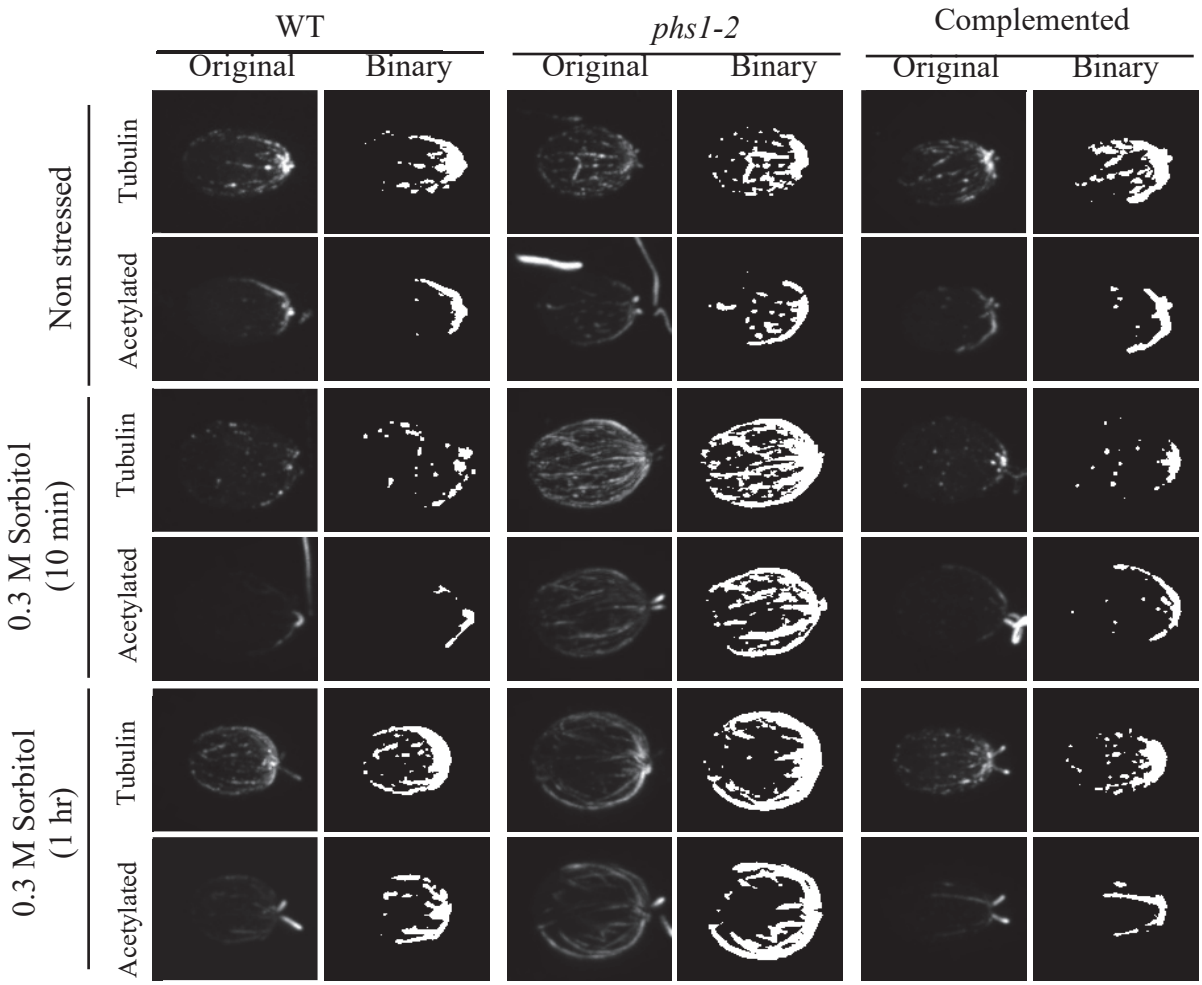

Figure 24: Original fluorescence images and the corresponding binary images by Image J of *Chlamydomonas* cells under 0 and 0.3 M sorbitol.

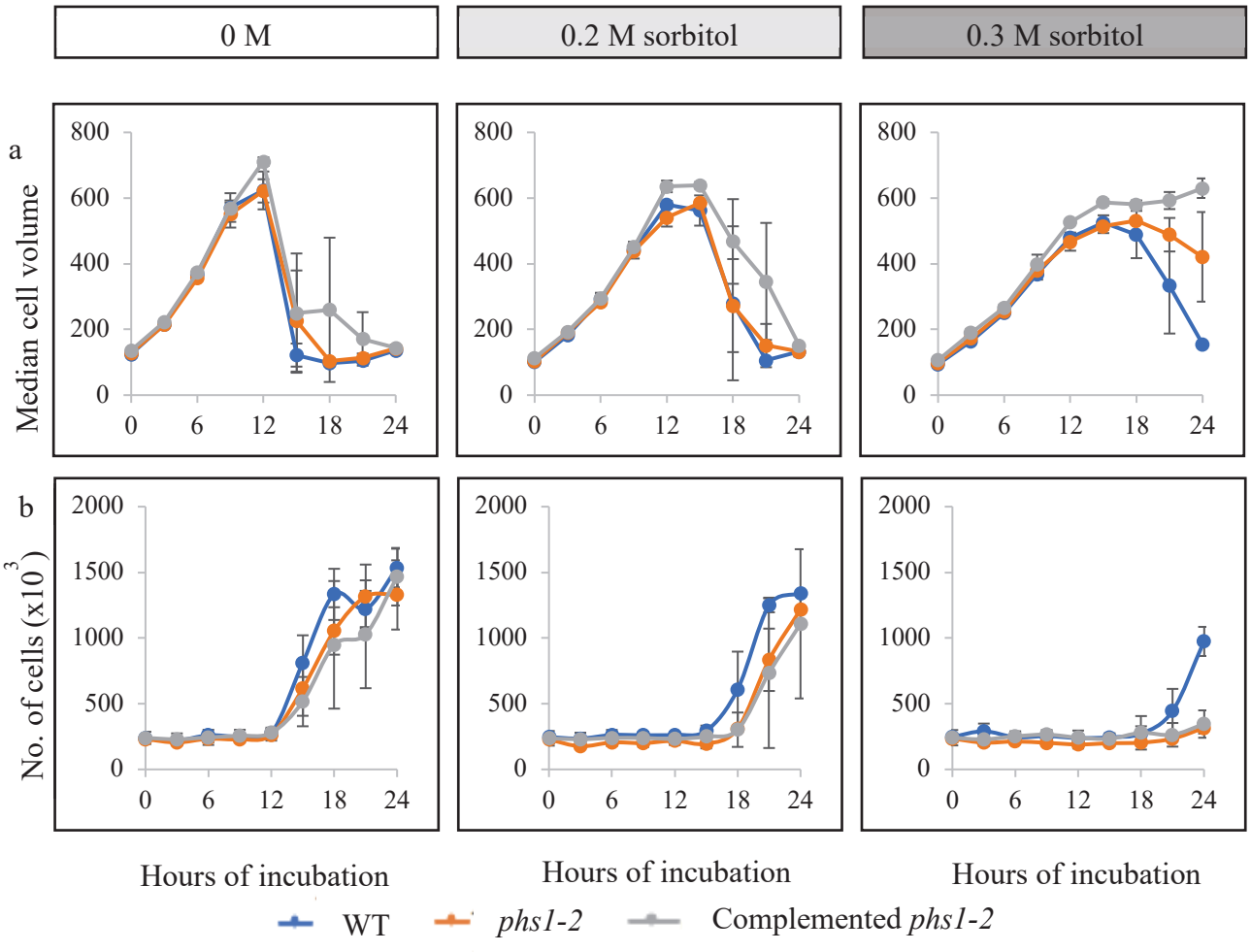
0 M
0.2 M sorbitol
0.3 M sorbitol
a
Median cell volume
800
600
400
200
0
0 6 12 18 24
b
No. of cells (x10^3)
2000
1500
1000
500
0
0 6 12 18 24
Hours of incubation
Hours of incubation
Hours of incubation
WT
phs1-2
Complemented phs1-2

c

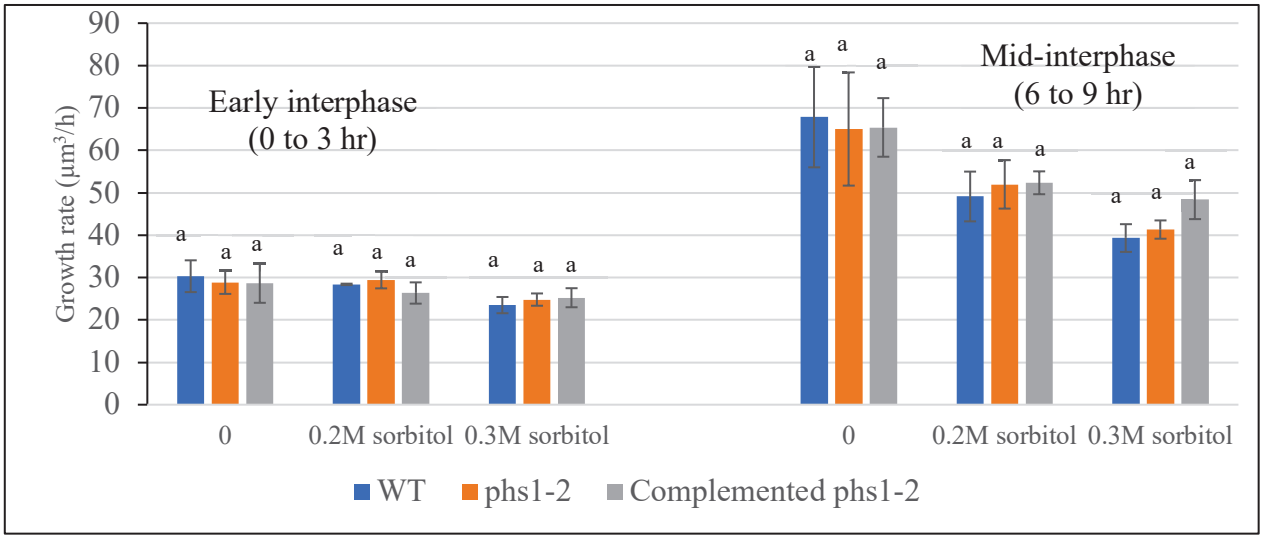

Figure 25: Sorbitol stress treatment in the early interphase of *Chlamydomonas* cells. Stress treatments were applied at the start of light period. (a) Median cell volume (b) number of cells of *Chlamydomonas* cells treated with 0, 0.2 M and 0.3 M sorbitol for 24 hours. (c) Growth rate of *Chlamydomonas* cells at the early interphase (0 to 3 hr after the start of light period) and mid interphase (6 to 9 hr after the start of light period). Error bars indicate of standard deviation for three biological replicates. Statistical analysis by using one-way ANOVA with Tukey HSD post-hoc test was performed, where p-value <0.05 indicates significantly different.

a

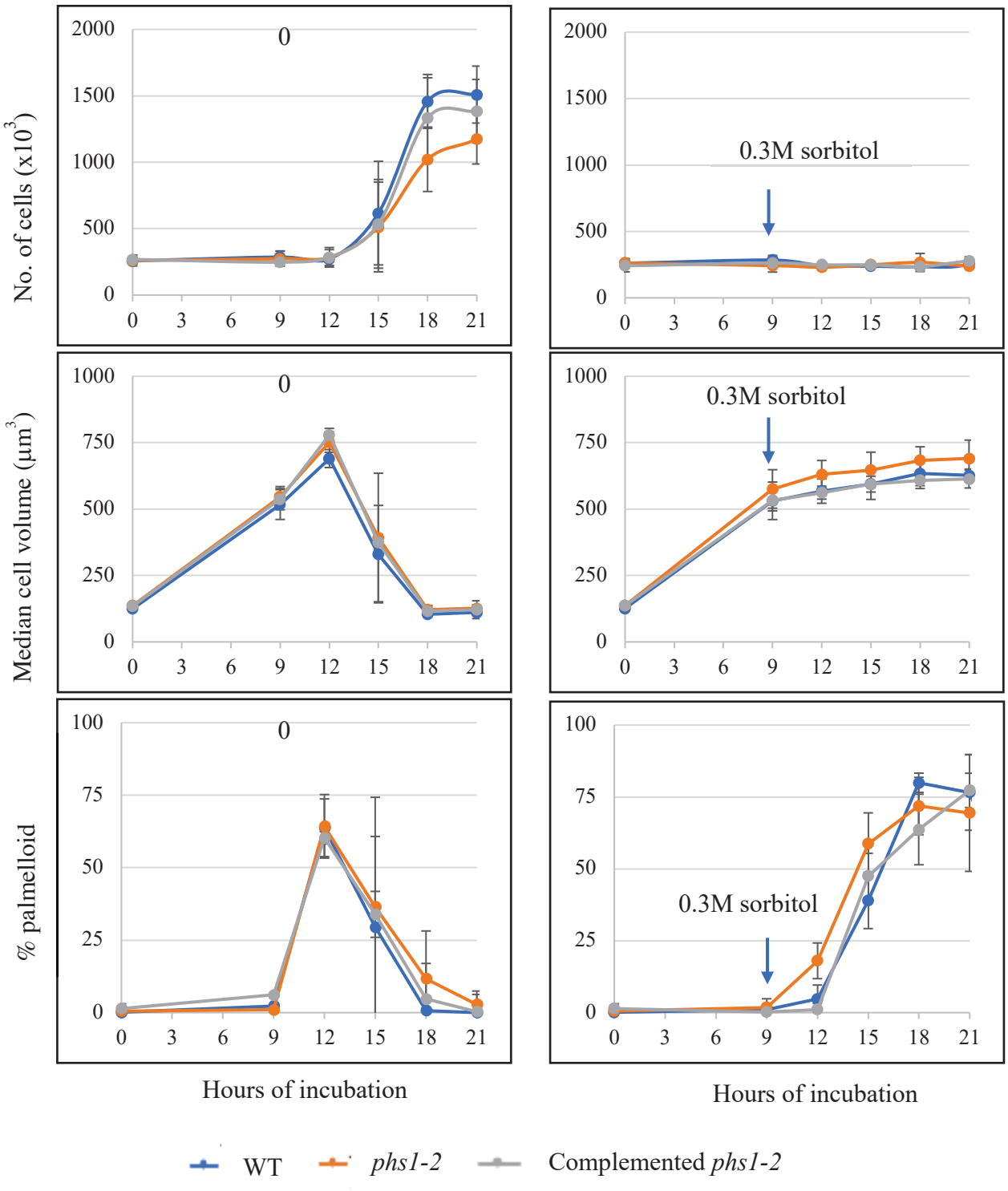
No. of cells (x10^3)
Median cell volume (µm^3)
% palmelloid
0
0.3M sorbitol
Hours of incubation
Hours of incubation
WT
phs1-2
Complemented phs1-2

b

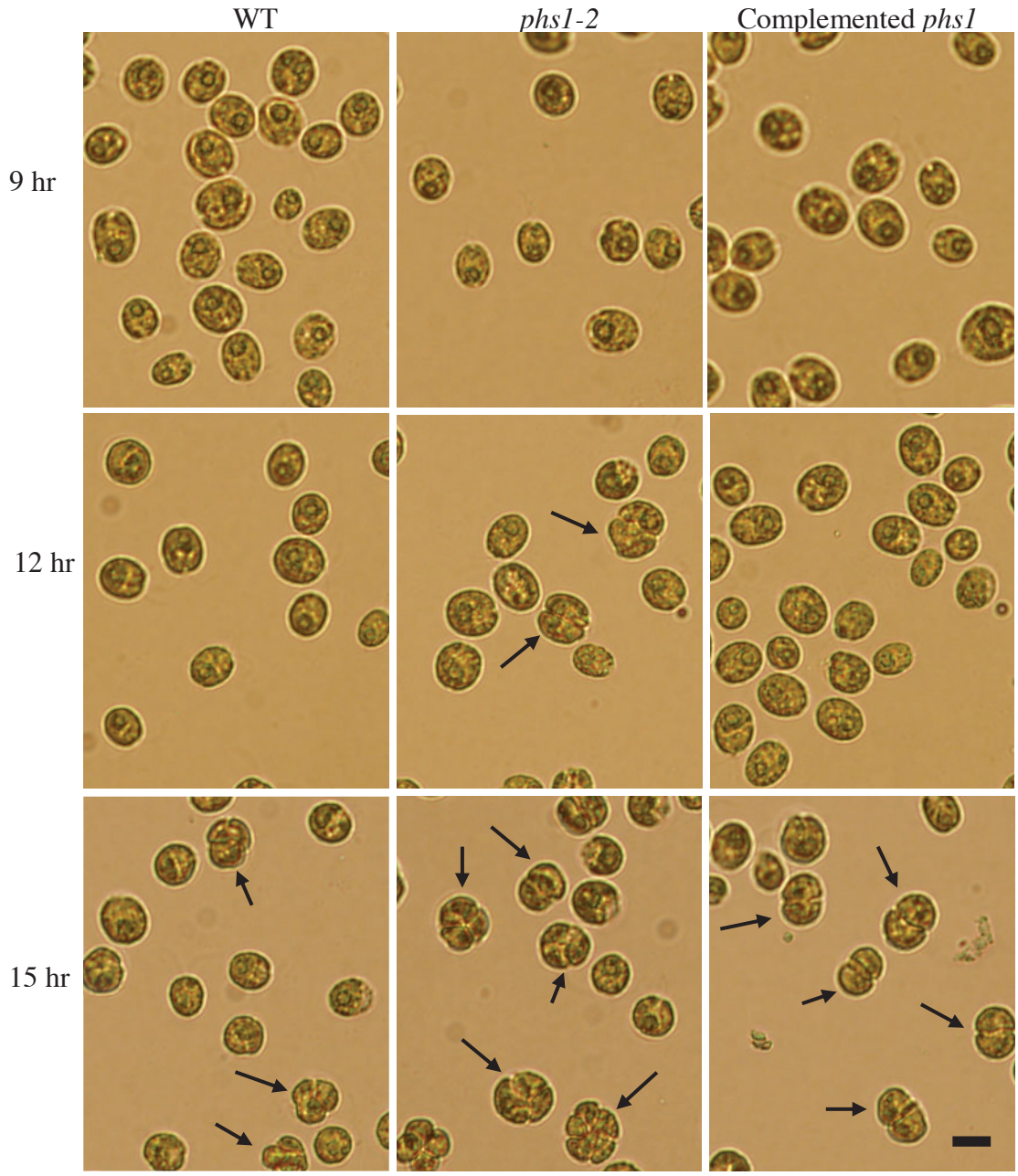

c

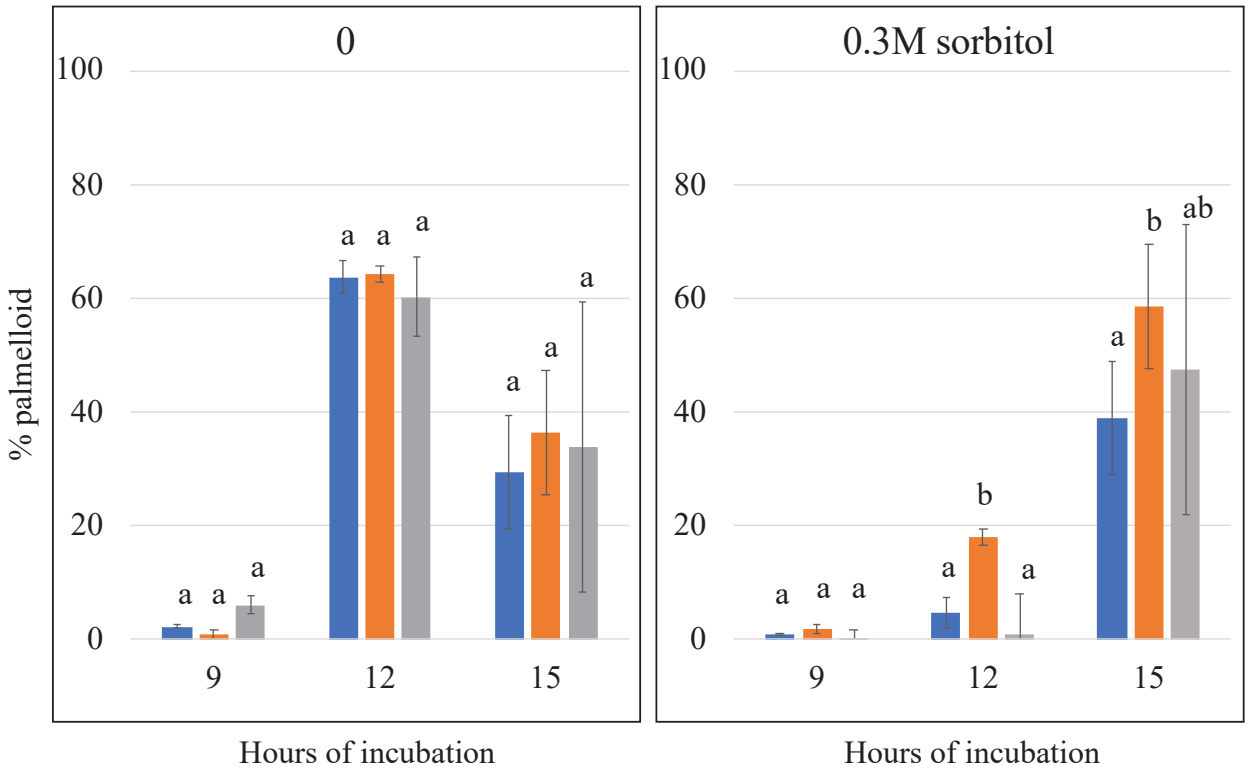

Figure 26: Sorbitol stress treatment in the late interphase of *Chlamydomonas* cells. Sorbitol treatments were applied to *Chlamydomonas* cells 9 hr after the start of light period. (a) Number of cells, median cell volume and percentage of palmelloids in *Chlamydomonas* cells treated with 0 and 0.3 M sorbitol. (b) Bright field microscopic images of *Chlamydomonas* cells treated with 0 and 0.3 M sorbitol at 9, 12 and 15 hr. Arrows indicate the formation of *Chlamydomonas* palmelloid. Bar indicates 10 µm. (c) Bar graph showed the percentage of palmelloids in *Chlamydomonas* at the 9, 12 and 15 hr with and without sorbitol stress treatment. Statistical analysis by using one-way ANOVA with Tukey HSD post-hoc test was performed, where p-value <0.01 indicates significantly different. Error bars indicates of standard deviation of five biological replicates.

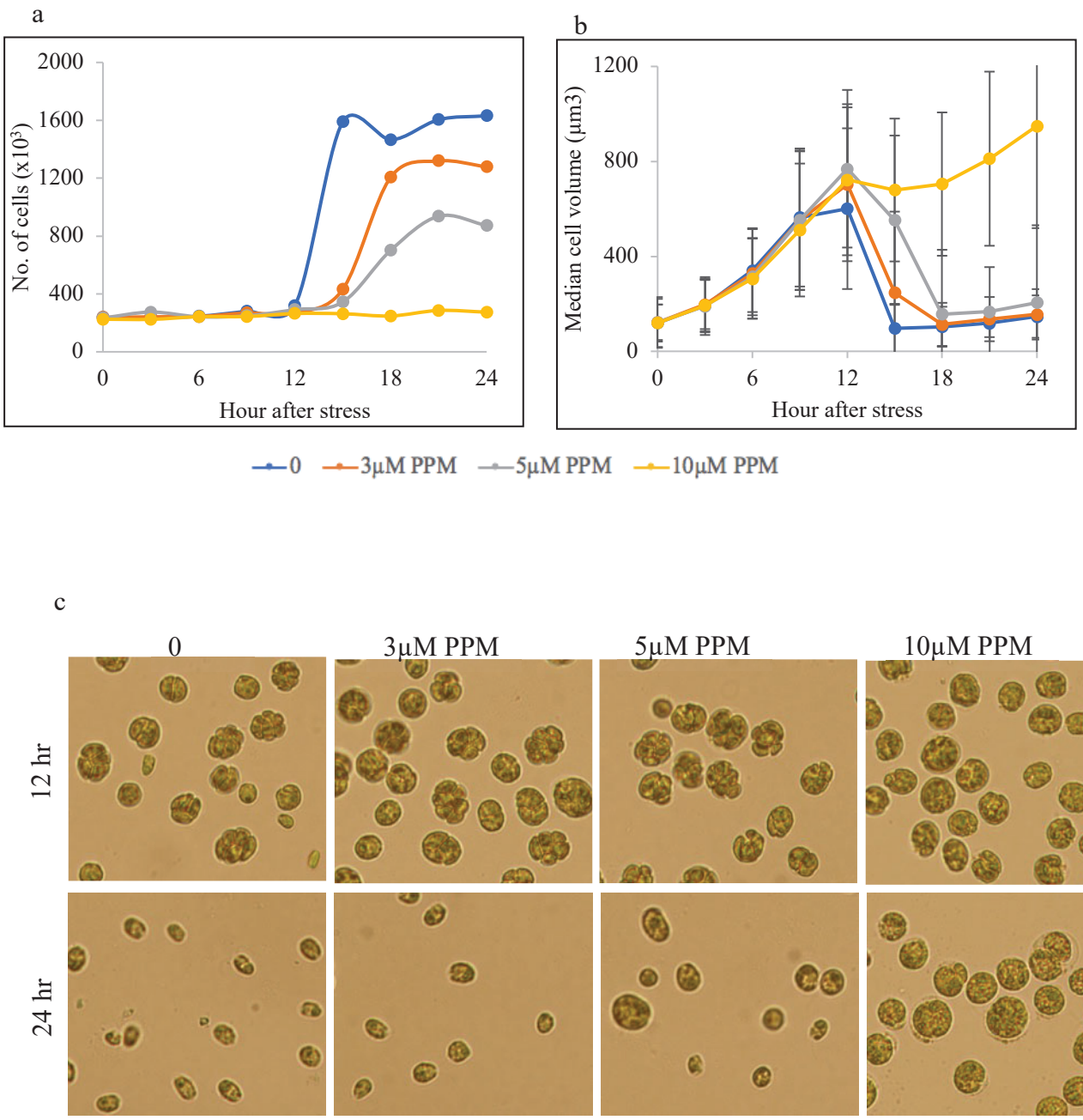

Figure 27: Propyzamide treatment on *Chlamydomonas* cells. *Chlamydomonas* cells were treated with propyzamide at the beginning of light period. (a) Number of cells, (b) median cell volume (c) bright field microscopic images of *Chlamydomonas* wild-type cells treated with 0, 3, 5 and 10 µM propyzamide (PPM). Error bars indicate of standard deviation for cells (n=~2000) in one biological sample.

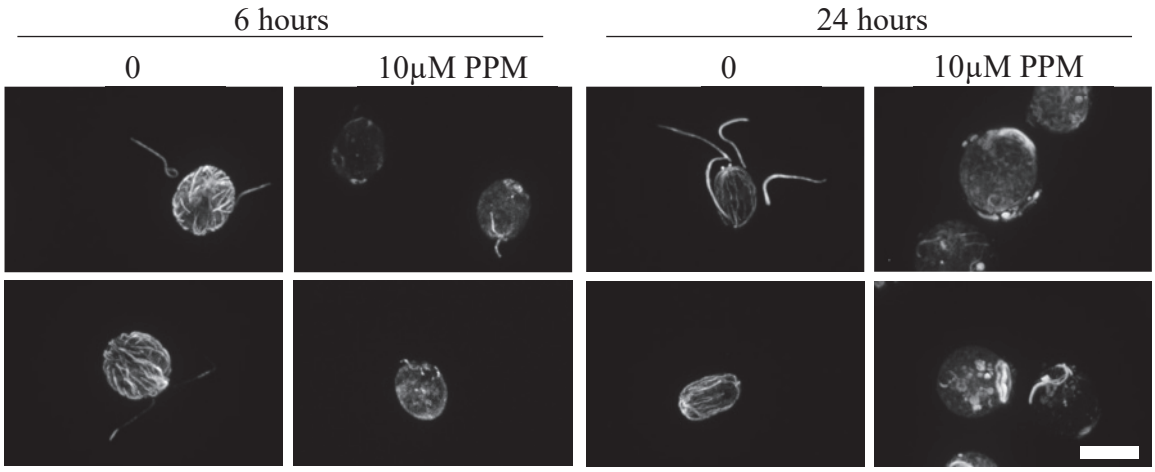

Figure 28: Microscopic images of *Chlamydomonas* cells after 6 hr and 24 hr in 10 μM propyzamide (PPM). Bar indicates 10 μm. No microtubules were observed in cells treated with PPM.

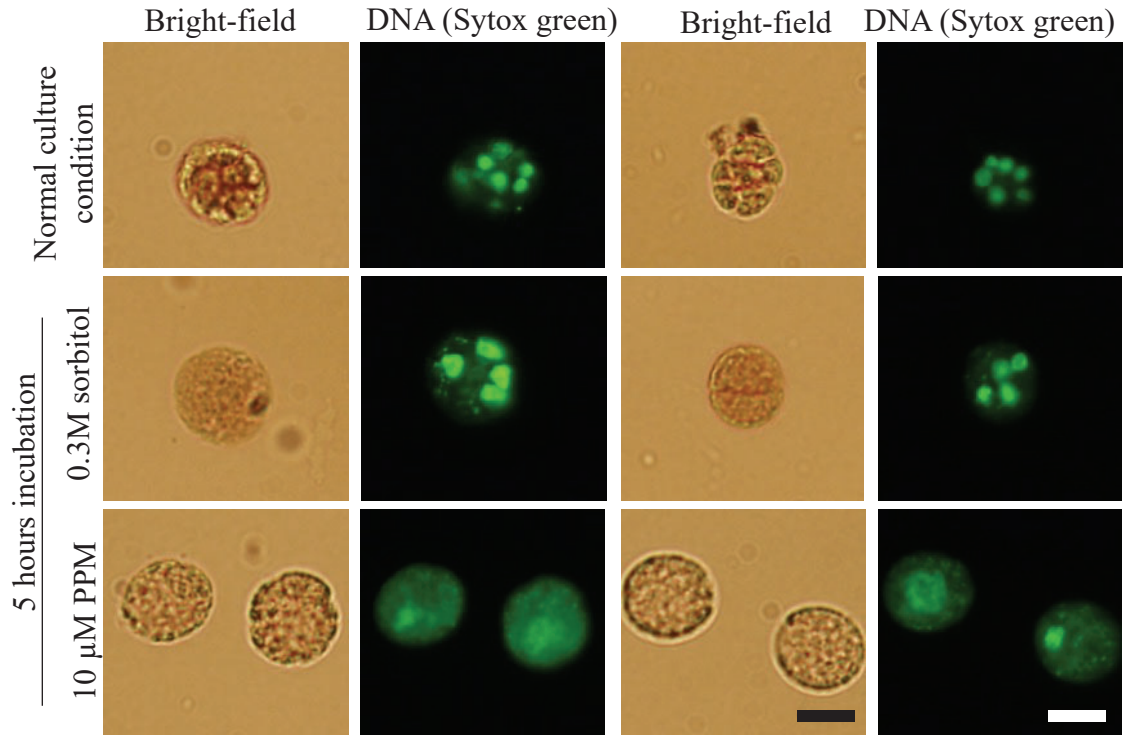

Figure 29: Bright-field and fluorescence microscopic images of *Chlamydomonas* cells with the application of stress treatments (0.3 M sorbitol and 10 μM PPM) at the late interphase (9 hr).

DISCUSSIONS

PHS1 genes in the plant lineage

A characteristic feature of the PHS1 structure is the presence of both a unique tubulin kinase domain and a MPK phosphatase-like domain in a single protein sequence. The tubulin kinase domain has a high sequence homology to the atypical kinase domain of the actin-fragmin kinases (which phosphorylate actin) found in slime molds, ciliates, and non-animal holozoans (Gettemans et al., 1992; Eichinger et al., 1996; Steinbacher et al., 1999). In PHS1, the tubulin kinase domain is situated between the N-terminal kinase interaction motif and the C-terminal phosphatase catalytic domain of a MPK phosphatase-like phosphatase. Since MPK phosphatases are ancient and are present all the eukaryotic organisms (Theodosiou and Ashworth, 2002), insertion of the atypical kinase domain into a MPK phosphatase of an ancient early plants, probably by the horizontal gene transfer from an ancient lower single-celled animal, likely represents a hallmark of the evolution of the plant-specific PHS1 tubulin kinase.

All the sequenced genomes of Rhodophyta (red algae) lack *PHS1*, whereas many (but not all) green algae (the Chlorophyta division) and all the subsequently evolved plants possess *PHS1* genes, indicating that *PHS1* evolved in Chlorophyta. The Chlorophyta green algae live in diverse environments, including marine, blackish water, and freshwater. Notably, all the freshwater green algae for which genomes are sequenced (including the Chlorophyceae class) possess apparently intact *PHS1* genes, while the two marine green algae, *Bathycoccus prasinos* (the Mamiellophyceae class) and *Dunaliella salina* (the Chlorophyceae class), do not show evidence of *PHS1* in their genomes. Since PHS1 is activated under the moderate salinity (such as 10% of sea water), marine habitat with constantly high salinity and high osmotic pressure may be detrimental to organisms possessing PHS1. We speculate that *PHS1* genes may have been lost in these marine-living organisms. A possible exception is the marine green algae *Micromonas pusilla* (the Mamiellophyceae class), in which a full length PHS1 is apparently encoded in its genome. We noted that two insertions of 17 and 41 amino acid residues are inserted into the *Micromonas* kinase domain, raising a possibility that the tubulin kinase activity is affected by the insertions. When the kinase domain of the *Arabidopsis* PHS1 was expressed in *E. coli* and purified, the recombinant kinase displayed a robust tubulin phosphorylation activity (unpublished results in the Hashimoto lab). Tubulin phosphorylation activities of recombinant PHS1 kinase domains from *Micromonas*

and other representative green algae need to be examined to show whether green algae PHS1s are functional tubulin kinases. As more genome sequences of green algae become available, possible association of PHS1 with freshwater habit will be challenged.

The proposal that presence of functional PHS1 may be unnecessary or even detrimental to plants habituating in environments with constant hyperosmotic stress presents an interesting avenue for future research. Some land plants have evolved to adapt to aquatic environments and complete their entire life cycles under water. For examples, during the early divergence of the monocot angiosperm lineages, the greater duck weed *Spirodela polyrhiza* (Japanese name; Ukikusa) adapted to aquatic freshwater whereas the seagrass *Zostera marina* (Japanese name; Amamo) became habituated in the sea. The genomes of these aquatic angiosperms are now available (An et al., 2019; Olsen et al., 2016) and offer opportunities to examine whether functional *PHS1* genes are present in freshwater and marine plants. The marine lifestyle of the seagrass caused the genomic losses of genes involved in stomata development, terpenoid biosynthesis, ethylene signaling, ultraviolet protection, and far-red sensing (Olsen et al., 2016).

Activation of PHS1 tubulin kinase

Thr349 of α-tubulin is specifically phosphorylated by *Arabidopsis* PHS1 *in planta* (Fujita et al., 2013). Phosphoproteomics in *Arabidopsis* seedlings revealed that this PHS1-target site is not or barely phosphorylated under unstressed conditions, but becomes increasingly phosphorylated after seedlings are dehydrated for up to 90 min (Umezawa et al., 2013) or are treated 5 min by 0.3M mannitol or 0.15M NaCl (Stecker et al., 2014). Phosphorylation of rice α-tubulins also becomes apparent after 5 min of 0.4M NaCl or 0.8M sorbitol treatment of rice seedling roots (Ban et al., 2013). Immunohistochemical analysis of *Arabidopsis* leaf epidermal cells showed that interphase cortical microtubules become more disassembled after 10 min of 0.8M sorbitol treatment, concomitant with increase of tubulin phosphorylation (Fujita et al., 2013). These results demonstrate that PHS1-mediated tubulin phosphorylation in angiosperms starts ca. 5 min after hyperosmotic stress and results in destabilization of interphase microtubule arrays.

In *Chlamydomonas*, I showed that PHS1 phosphorylates Thr349 of α-tubulin 10 min after application of >0.2M sorbitol in both interphase and mitotic cells, and causes fragmentation of interphase cytoplasmic microtubules after 10 min. Since the cytosolic osmolarity of *Chlamydomonas* cells is approximately 170 mosM (Komsic-Buchmann et al., 2014), this response

is caused by mild hyperosmotic stress. Although mitotic microtubule arrays were not examined in my study, due to technical difficulties using confocal microscopy, mitotic arrays are likely destabilized by rapid tubulin phosphorylation. It appears that activation of PHS1 tubulin kinase activity occurs both in interphase and mitotic cells immediately upon hyperosmotic stress.

I showed that stress-induced tubulin phosphorylation is transient, even when osmotic stress persists; in the continuous presence of >0.2M sorbitol, phosphorylated *Chlamydomonas* tubulins are mostly de-phosphorylated after 1 hr in interphase cells and after 3 hr in mitotic cells. We do not know what causes the observed differences in the steady-state levels of phosphorylated tubulins under continuous stress during the cell cycle. In *Arabidopsis* seedlings, sorbitol-induced tubulin phosphorylation levels dramatically decrease after several hours of continuous stress (unpublished results of the Hashimoto lab). De-activation (or de-sensitization) of the PHS1 tubulin kinase, as commonly observed for stress-activated MPKs (Muzzey et al., 2009), increased activity of putative tubulin de-phosphatases during continuous stress, or both, may be responsible for this phenomena.

Previous studies showed that Thr349 of α-tubulin is phosphorylated by stresses caused either by salt (NaCl) or osmotic agents (mannitol or sorbitol) (Ban et al., 2013; Fujita et al., 2013; Stecker et al., 2014). Since salt stress to plants involves both ionic imbalance and hyperosmotic effects (Verslues et al., 2006), I compared the effects of NaCl and sorbitol at the equivalent morality, and found that tubulin phosphorylation is mainly triggered by hyperosmotic stress, whereas NaCl inhibits cell growth strongly by ionic imbalance. Sensing mechanisms of salinity and osmotic stress are distinct in plants, but the molecular identities of responsible sensors and receptors are still largely elusive (Lamers et al., 2020).

Hyperosmotic stress responses in *Chlamydomonas*

Responses of *Chlamydomonas* cells to salinity stress (a combination of hyperosmotic and ionic stresses) have been studied (reviewed by Shetty et al., 2019), and include alterations in morphology (Khona et al., 2016), photobiology (Neelam and Subramanyan, 2013), transcriptomes (Wang et al., 2018), proteomes (Sithtisarn et al., 2017), and plus-end dynamics of cytoplasmic microtubules (Liu et al., 2017). Relevant studies on hyperosmotic stress are very limited; to my knowledge, only one study reports metabolomics changes of *Chlamydomonas* cells to hyperosmotic stress after 5 hr (Tietel et al., 2020).

In my study, I found that hyperosmotic stress causes PHS1-mediated transient tubulin phosphorylation and microtubule destabilization, as well as formation of multicellular aggregates known as "palmelloids". Palmelloids in *Chlamydomonas* and related green algae are encapsulated in the mucilage rich in acidic polysaccharides (Crayton, 1982) and hydroxyproline-containing glycoproteins (Miller et al., 1974). Palmelloid formation is caused by various environmental stresses (de Carpentier et al., 2019), including salinity (e.g., Khona et al., 2016). Although physiological roles of palmelloids are not well known, it has been proposed that formation of large cell aggregates enables the algal cells to better escape herbivory from grazing zooplanktons (Lurling and Beekman, 2006).

Possible roles of PHS1-mediated microtubule destabilization

The spindle assembly checkpoint (SAC) in yeast and animals (Opisthokonts) functions as a surveillance mechanisms to ensure equal segregation of chromosomes during cell division, by arresting metaphase until all chromosomes are correctly attached to spindle microtubules (London and Biggins, 2014). Land plants and green algae possess both shared and unique cell cycle control components (Komaki and Schnittger, 2016), and display highly compromised SAC responses. When spindle microtubules were not formed by treating *Arabidopsis* roots with a high dosage (1 μM) of oryzalin, a microtubule depolymerizing drug, metaphase cells were transiently arrested but re-initiated the cell cycle after ~2 hr without subsequent cell division to attain polyploidy (Komaki and Schnittger, 2016). DNA re-replication was also observed in *Chlamydomonas* cells when treated with a high dosage of the microtubule-depolymerizing drug amiprophos-methyl for a prolonged duration or disrupted in genes involved in tubulin folding chaperones or a microtubule nucleation (Tulin and Cross, 2014). I also observed a large undivided nucleus in an enlarged *Chlamydomonas* cell treated with 10 μM propyzamide for >6 hr. Thus, disruption of mitotic microtubules in land plants and green algae does not prevent progression of the cell cycle due to inefficient SAC functions.

Effects of hyperosmotic stress on mitotic microtubules are expected to be transient and subtle. Moderate destabilization of mitotic microtubules by lower dosages of oryzalin (<0.2 μM) delayed the progression of mitosis in *Arabidopsis* roots in a SAC-dependent manner (Komaki and Schnittger, 2017). In *Chlamydomonas* cells, I found that the cell cycle progression was delayed by treatment of propyzamide at 3 and 5 μM. Hyperosmotic stress by 0.3 M sorbitol might cause

sufficient microtubule destabilization that would result in the cell cycle delay in *Chlamydomonas* cells. However, hyperosmotic stress also induced formation of un-hatched palmelloids, which made the analysis of newly formed daughter cells challenging. Due to PHS1 activation is only lasted for a relatively short period of time, approximately 1 hour after the stress treatment, the immediate biological response in *Chlamydomonas* will be the main focus of this study. My studies revealed that PHS1 might played a role in the delayed of cell cycle progression in *Chlamydomonas* under osmotic stress condition.

During interphase, hyperosmotic stress-triggered transient microtubule destabilization does not affect cell growth (the rate of cell volume increase). What roles might the PHS1-mediated microtubule destabilization have for cellular responses to hyperosmotic stress, and what would be future research projects to decipher elusive PHS1 functions, specifically in *Chlamydomonas* cells? I will discuss here possible roles of PHS1 in the interphase algal cells.

In land plants, interphase microtubules are anchored to the inner face of the plasma membrane, and guide the movement of the cellulose synthase complexes, thereby controlling the direction of cell expansion (Paredez et al., 2006). In contrast, cell wall of *Chlamydomonas* cells are composed of non-cellulosic polysaccharides (Adair and Snell, 1990), with no firm evidence of cellulose fibrils in the wall. *Chlamydomonas* interphase microtubules in the cell body are characterized of four microtubule bundles, called rootlets (two bundles composed of four microtubules, whereas the other two having two microtubules) containing acetylated tubulins, called microtubule rootlet (Cross and Umen, 2015). The microtubule rootlets are nucleated from the basal cell body and extend basally along the cell periphery. Roles of these microtubule bundles are not fully understood, but one function is to position the eyespot, a light-sensitive organelle that confers phototaxes toward light (Harris, 2009). The eyespot is invariably associated at the equator of the cell with one of the rootlet, called the daughter four-membered (D4) rootlet, which is noticeably longer and more acetylated than the other rootlets (Mittelmeier et al., 2011). Cell biological analyses of several eyespot-positioning mutants suggest that the length of the D4 rootlet is the major determinant of eyespot positioning (Boyd et al., 2011). However, cold-induced microtubule depolymerization experiments in interphase cells indicate that, once positioned, microtubules become no longer necessary to remain the eyespot at a fixed cellular location (Boyd et al., 2011). Thus, to influence the eyespot positioning, hyperosmotic stress must be applied at the exact moment in the cell cycle when the eyespot and the microtubule rootlets assemble de novo

after cell division; most interphase periods are likely insensitive.

Another known function of the four-membered rootlets is to foretell the position where the cleavage furrow will form during cytokinesis (Witman, 2008), as much a similar way that the microtubule preprophase band predicts the cellular location where the phragmoplast microtubule array will form during anaphase in land plants. In this case as well, hyperosmotic stress may be able to affect the assembly and organization of the microtubule rootlets only during a short time window at the beginning of the interphase.

Flagella are shortened immediately before prophase and eventually adsorbed, while new flagella are formed after completion of cytokinesis (Cross and Umen, 2015). Tubulins are delivered to and recovered from the tip of a growing or shrinking flagellum by the intraflagellar transport machinery (Prevo et al., 2017). Microtubules in flagella are highly stable and are strongly labelled by an anti-acetyltubulin antibody. It is not known whether the phosphorylated tubulin can serve as a cargo of the intraflagellar transport motors, but I have not observed apparent flagellar phenotypes upon hyperosmotic stress.

Defensive and stress-responsive roles of the plant microtubule cytoskeleton are still largely elusive. Recent studies reveal that several pathogens deliver effector proteins into host cells to disrupt stabilization and organization of interphase microtubules (Bhandari and Brandizzi, 2020). Although intact microtubule organization is apparently important for resistance to pathogens, how microtubule stability contributes to immunity is not known. Several intracellular signaling proteins, such as a ROP GTPase activating protein (Hoefle et al., 2011) and a psudokinase (Mahdi et al., 2020), are dynamically associated with cortical microtubules, indicating their roles as a signaling scaffold. Future studies on PHS1-mediated hyperosmotic stress-induced microtubule destabilization will lead to better understanding on the emerging regulatory functions of plant microtubules to biotic and abiotic stresses.

ACKNOWLEDGEMENT

There are many people I would like to thank who have helped me in completing my thesis. First and foremost, I would like to deliver my deepest appreciation to my supervisor, Prof. Takashi Hashimoto for giving his guidance, advice and encouragement in my research. Prof. Hashimoto had been very supportive in helping and guiding me to complete my doctoral thesis.

I am particularly grateful to assistant professor, Dr. Shinichiro Komaki, for his valuable guidance, help and support in my research. Dr. Komaki had been providing lots of advice and support in experimental and data analysis in my research. I would also like to deliver my appreciation to Dr. Takehide Kato and Dr. Hideyuki Takahashi for their advice, support and encouragement throughout my project. Thanks and appreciation also extended to all Plant Cell Function Lab members.

I would like to extend my appreciations to my committee members, Prof. Masaaki Umeda from Plant Growth Regulation Lab and Prof. Toshiro Ito from Plant Stem Cell Regulation and Floral Patterning Lab. Their valuable advice and guidance had helped me to in completing my thesis.

Many thanks also go to Prof. Hideya Fukuzawa and Dr. Takashi Yamano from Kyoto University for their guidance and advice in *Chlamydomonas* study especially on transformation and microscopy experiments. I am also thankful to Dr. Bo Liu and his lab members from University of California, Davis for their guidance and advice on immunofluorescence microscopy technique.

My deepest appreciation belongs to my beloved family, my parents, sisters and my fiancée, Foong Choon Pin. They always encourage and support me throughout my study. Their encouragement had motivated me in completing my study.

Finally, I would like to deliver my appreciation to NAIST International Scholarship Program, School of Biological Sciences, NAIST and Hashimoto Lab for the financial support.

REFERENCES

Achard, P., Cheng, H., De Grauwe, L., Decat, J., Schoutteten, H. et al. (2006). Integration of plant responses to environmentally activated phytohormonal signals. Science 311(5757), 91-94.

Achard, P., Gusti, A., Cheminant, S., Alioua, M., Dhondt, S. et al. (2009). Gibberellin signaling controls cell proliferation rate in *Arabidopsis*. Curr. Biol. 19(14), 1188-1193.

Adair, W.S., and Snell, W.J. (1990) The *Chlamydomonas reinhardtii* cell wall: structure, biochemistry and molecular biology. In: Organization and Assembly of Plant and Animal Extracellular Matrix (R.P. Mecham and W.S. Adair, Eds.), Academic Press, Orlando, pp. 15-84.

Al-Bassam, J., and Corbett, K. D. (2012). α-Tubulin acetylation from the inside out. PNAS 109(48), 19515-19516.

An, D., Zhou, Y., Changsheng, L., Xiao, Q., Wang, T., et al. (2019) Plant evolution and environmental adaptation unveiled by long-read whole-genome sequencing of *Spirodela*. PNAS 116, 18893-18899.

Ban, Y., Kobayashi, Y., Hara, T., Hamada, T., Hashimoto, T. et al. (2013). α-tubulin is rapidly phosphorylated in response to hyperosmotic stress in rice and *Arabidopsis*. Plant Cell Physiol 54(6), 848-858.

Berthold, P., Schmitt, R., & Mages, W. (2002). An engineered Streptomyces hygroscopicus aph 7" gene mediates dominant resistance against hygromycin B in *Chlamydomonas reinhardtii*. Protist 153(4), 401.

Bhandari, D.D., and Brandizzi, F. (2020) Plant endomembranes and cytoskeleton: moving targets in immunity. Curr. Opin. Plant Biol. 58: 8-16.

Boyd, J.S., Gray, M.M., Thompson, M.D., Horst, C.J., and Dieckmann, C.L. (2011) The daughter four-membered microtubule rootlet determines anterior-posterior positioning of the eyespot in *Chlamydomonas reinhardtii*. Cytoskeleton 68: 459-469.

Bisova, K., Krylov, D. M., and Umen, J. G. (2005). Genome-wide annotation and expression profiling of cell cycle regulatory genes in *Chlamydomonas reinhardtii*. Plant Physiol 137(2), 475-491.

Carlier, M. F., Hill, T. L., and Chen, Y. (1984). Interference of GTP hydrolysis in the mechanism of microtubule assembly: an experimental study. PNAS 81(3), 771-775.

Cassimeris, L. (1993). Regulation of microtubule dynamic instability. Cytoskeleton 26(4), 275-281.

Chernys, J. T., and Zeevaart, J. A. (2000). Characterization of the 9-cis-epoxycarotenoid dioxygenase gene family and the regulation of abscisic acid biosynthesis in avocado. Plant Physiol 124(1), 343-354.

Claeys, H., De Bodt, S., and Inzé, D. (2014). Gibberellins and DELLAs: central nodes in growth regulatory networks. Trends Plant Sci. 19(4), 231-239.

Conde, A., Chaves, M. M., and Gerós, H. (2011). Membrane transport, sensing and signaling in plant adaptation to environmental stress. Plant Cell Physiol 52(9), 1583-1602.

Crayton, M.A. (1982) A comparative cytochemical study of *Vovocacean* matrix polysaccharides. J. Phycol. 18: 336-344.

Cross, F. R., and Umen, J. G. (2015). The *Chlamydomonas* cell cycle. Plant J 82(3), 370-392.

Cueva, J. G., Hsin, J., Huang, K. C., and Goodman, M. B. (2012). Posttranslational acetylation of α-tubulin constrains protofilament number in native microtubules. Curr. Biol. 22(12), 1066-1074.

De Carpentier, F., Lemaire, S.D., and Danon, A. (2019) When unity is strength: the strategies used by *Chlamydomonas* to survive environmental stresses. Cells 8: 1307.

Eichinger, L., Bomblies, L., Vandekerckhove, J., Schleicher, M., and Gettemans, J. (1996). A novel type of protein kinase phosphorylates actin in the actin-fragmin complex. EMBO J. 15: 5547–5556.

Erickson, H. P., and O'Brien, E. T. (1992). Microtubule dynamic instability and GTP hydrolysis. Annu Rev Bioph Biom 21(1), 145-166.

Ermilova, E. (2020). Cold Stress Response: An Overview in *Chlamydomonas*. Front. Plant Sci. 11, 1364.

Flavin, M., and Slaughter, C. (1974). Microtubule assembly and function in *Chlamydomonas*: inhibition of growth and flagellar regeneration by antitubulins and other drugs and isolation of resistant mutants. J. Bacteriol 118(1), 59-69.

Fujita, S., Pytela, J., Hotta, T., Kato, T., Hamada, T. et al. (2013). An atypical tubulin kinase mediates stress-induced microtubule depolymerization in *Arabidopsis*. Curr. Biol. 23(20), 1969-1978.

Gao, X. H., Xiao, S. L., Yao, Q. F., Wang, Y. J., and Fu, X. D. (2011). An updated GA signaling 'relief of repression'regulatory model. Molecular Plant 4(4), 601-606.

Garz, A., Sandmann, M., Rading, M., Ramm, S., Menzel, R., and Steup, M. (2012). Cell-to-cell diversity in a synchronized *Chlamydomonas* culture as revealed by single-cell analyses. Biophys. J. 103(5), 1078-1086.

Gettemans, J., De Ville, Y., Vandekerckhove, J., and Waelkens, E. (1992). Physarum actin is phosphorylated as the actin-fragmin complex at residues Thr203 and Thr202 by a specific 80 kDa kinase. EMBO J. 11: 3185–3191.

Goddard, R. H., Wick, S. M., Silflow, C. D., and Snustad, D. P. (1994). Microtubule components of the plant cell cytoskeleton. Plant Physiol. 104(1), 1.

Grossman, A. R. (2007). The *Chlamydomonas* genome reveals the evolution of key animal and plant functions. Science 318(5848), 245-250.

Harris, E.H. (2009) The *Chlamydomonas* Sourcebook, Volume 1, second edition. Chapter 2; Cell architecture., Elsevier, Oxford, pp. 60-64.

Harris, J. A., Liu, Y., Yang, P., Kner, P., and Lechtreck, K. F. (2016). Single-particle imaging reveals intraflagellar transport–independent transport and accumulation of EB1 in *Chlamydomonas* flagella. Mol. Biol. Cell 27(2), 295-307.

Hashimoto, T. (2015). Microtubules in plants. The *Arabidopsis* Book, e0179.

Hauvermale, A. L., Ariizumi, T., and Steber, C. M. (2012). Gibberellin signaling: a theme and variations on DELLA repression. Plant Physiol 160(1), 83-92.

Heifetz, P. B., Förster, B., Osmond, C. B., Giles, L. J., and Boynton, J. E. (2000). Effects of Acetate on Facultative Autotrophy in *Chlamydomonas reinhardtii* Assessed by Photosynthetic Measurements and Stable Isotope Analyses. Plant Physiol 122(4), 1439-1446.

Hoefle, C., Huesmann, C., Schultheiss, H., Börnke, F., Hensei, G., et al. (2011) A barley ROP GTPase activating protein associates with microtubules and regulates entry of the barley powdery mildew fungus into leaf epidermal cells. Plant Cell 23: 2422-2439.

Holmes, J. A., and Dutcher, S. K. (1989). Cellular asymmetry in *Chlamydomonas reinhardtii*. J. Cell Sci. 94(2), 273-285.

Hotta, T., Fujita, S., Uchimura, S., Noguchi, M., Demura, T. et al. (2016). Affinity purification and characterization of functional tubulin from cell suspension cultures of *Arabidopsis* and tobacco. Plant Physiol. 170(3), 1189-1205.

Janke, C., and Bulinski, J. C. (2011). Post-translational regulation of the microtubule cytoskeleton: mechanisms and functions. Nat. Rev. Mol. Cell Biol. 12(12), 773.

Huang, B., Piperno, G., and Luck, D. J. (1979). Paralyzed flagella mutants of *Chlamydomonas reinhardtii.* Defective for axonemal doublet microtubule arms. J. Biol. Chem. 254(8), 3091-3099.

Kato, Y., Ho, S. H., Vavricka, C. J., Chang, J. S., Hasunuma, T., et al. (2017). Evolutionary engineering of salt-resistant *Chlamydomonas* sp. strains reveals salinity stress-activated starch-to-lipid biosynthesis switching. Bioresour. Technol 245, 1484-1490.

Khona, D.K., Shirolikar, S.M., Gawde, K.K., Hom, E., Deodhar, M.A., et al. (2016) Characterization of salt stress-induced palmelloids in the green algae, *Chlamydomonas reinhardtii*. Algal Res. 16: 434-448.

Komaki, S., and Schnittger, A. (2016) The spindle checkpoint in plants – a green variation over a conserved theme. Curr. Opin. Plant Biol. 34: 84-91.

Komaki, S., and Schnittger, A. (2017). The spindle assembly checkpoint in *Arabidopsis* is rapidly shut off during severe stress. Dev. Cell 43(2), 172-185.

Komsic-Buchmann, K., Wüstehoff, L., and Becker, B. (2014) The contractile vacuole as a key regulator of cellular water flow in *Chlamydomonas reinhardtii*. Eukaryotic Cell 13: 1421-1430.

Kubo, T., Hou, Y., Cochran, D. A., Witman, G. B., and Oda, T. (2018). A microtubule-dynein tethering complex regulates the axonemal inner dynein f (I1). Mol. Biol. Cell 29(9), 1060-1074

Lamers, J., van der Meer, T., and Testerink, C. (2020) How plants sense and respond to stressful environments. Plant Physiol. 182: 1624-1635.

Johnson, K. A. (1998). The axonemal microtubules of the *Chlamydomonas* flagellum differ in tubulin isoform content. J. Cell Sci. 111(3), 313-320.

Jordan, M. A., and Wilson, L. (2004). Microtubules as a target for anticancer drugs. Nat. Rev. Cancer 4(4), 253.

Jordan, M. A., Toso, R. J., Thrower, D., and Wilson, L. (1993). Mechanism of mitotic block and inhibition of cell proliferation by taxol at low concentrations. PNAS 90(20), 9552-9556.

Jordan, M. A., Thrower, D., and Wilson, L. (1992). Effects of vinblastine, podophyllotoxin and nocodazole on mitotic spindles. Implications for the role of microtubule dynamics in mitosis. J. Cell Sci. 102(3), 401-416.

Kinoshita, E., Kinoshita-Kikuta, E., Takiyama, K., and Koike, T. (2006) Phosphate-binding tag, a new tool to visualize phosphorylated proteins. Mol. Cell. Proteomics 5: 749-757.

L'Hernault, S. W., and Rosenbaum, J. L. (1985). *Chlamydomonas* alpha.-tubulin is posttranslationally modified by acetylation on the. epsilon.-amino group of a lysine. Biochem 24(2), 473-478.

LeDizet, M., and Piperno, G. (1986). Cytoplasmic microtubules containing acetylated alpha-tubulin in *Chlamydomonas reinhardtii*: spatial arrangement and properties. J. Cell Biol. 103(1), 13-22.

Li, L., and Yang, X. J. (2015). Tubulin acetylation: responsible enzymes, biological functions and human diseases. Cell. Mol. Life Sci. 72(22), 4237-4255.

Li, X., Patena, W., Fauser, F., Kinkerson, R.E., Saroussi, S., et al. (2019) A genome-wide algal mutant library and functional screen identifies genes required for eukaryotic photosynthesis. Nat. Genet. 31: 627-635.

Liu, Y., Visetsouk, M., Mynlieff, M., Qin, H., Lechtreck, K. F., et al. (2017). H+-and Na+-elicited rapid changes of the microtubule cytoskeleton in the biflagellated green alga *Chlamydomonas*. eLife, 6, e26002.

London, N., and Biggins, S. (2014) Signalling dynamics in the spindle checkpoint response. Nat. Rev. Mol. Cell Biol. 15: 736-747.

Lurling, M., and Beekman, W. (2006) Palmelloids formation in *Chlamydomonas reinhardtii*: defense against rotifer predators? Ann. Limnol. – Int. J. Lim. 42: 65-72.

Mahdi, L.K., Huang, M., Zhang, X., Nakano, R.T., Kopp, L,B., et al. (2020) Discovery of a family of mixed lineage kinase domain-like proteins in plants and their role in innate immune signaling. Cell Host Microbe 28: 813-826.

Maruta, H., Greer, K., and Rosenbaum, J. L. (1986). The acetylation of alpha-tubulin and its relationship to the assembly and disassembly of microtubules. J. of Cell Biol. 103(2), 571-579.

Mittelmeier, T. M., Boyd, J. S., Lamb, M. R., and Dieckmann, C. L. (2011). Asymmetric properties of the *Chlamydomonas reinhardtii* cytoskeleton direct rhodopsin photoreceptor localization. J. Cell Biol. 193(4), 741-753.

Meng, D., and Pan, J. (2016). A NIMA-related kinase, CNK4, regulates ciliary stability and length. Mol. Biol. Cell 27(5), 838-847.

Merchant, S. S., Prochnik, S. E., Vallon, O., Harris, E. H., Karpowicz, S. J., et al. (1993). Cloning of flagellar genes in *Chlamydomonas reinhardtii* by DNA insertional mutagenesis. Genetics, 135(2), 375-384.

Miller, D. H., Mellman, I. S., Lamport, D. T. A., and Miller, M. (1974) The chemical composition of the cell wall of *Chlamydomonas* gymnogama and the concept of a plant cell wall protein. J. Cell Biol. 63: 420-429.

Minai, L., Wostrikoff, K., Wollman, F. A., and Choquet, Y. (2006). Chloroplast biogenesis of photosystem II cores involves a series of assembly-controlled steps that regulate translation. Plant Cell 18(1), 159-175.

Mitchison, T., and Kirschner, M. (1984). Dynamic instability of microtubule growth. Nature 312(5991), 237.

Mohanta TK, Mishra AK, Khan A, Hashem A, Abd_Allah EF, Al-Harrasi A. Gene Loss and Evolution of the Plastome. Genes 2020; 11(10):1133.

Monk, B.C., Adair, W.S., Cohen, R.A., and Goodenough, U.W. (1983) Topography of *Chlamydomonas*: fine structure and polypeptide components of the gametic flagellar membrane surface and the cell wall. Planta 158: 517-533.

Muzzey, D., Gomez-Uribe, C.A., Mettetal, J.T., and van Oudenaarden, A. (2009) A systems-level analysis of perfect adaptation in yeast osmoregulation. Cell 138: 160-171.

Nakajima, K., Furutani, I., Tachimoto, H., Matsubara, H., and Hashimoto, T. (2004). SPIRAL1 encodes a plant-specific microtubule-localized protein required for directional control of rapidly expanding *Arabidopsis* cells. Plant Cell 16(5), 1178-1190.

Naoi, K., and Hashimoto, T. (2004). A semidominant mutation in an *Arabidopsis* mitogen-activated protein kinase phosphatase-like gene compromises cortical microtubule organization. Plant Cell, 16(7), 1841-1853.

Neelam, S., and Subramanyam, R. (2013). Alteration of photochemistry and protein degradation of photosystem II from *Chlamydomonas reinhardtii* under high salt grown cells. J. Photochem. Photobiol. B, Biol. 124, 63-70.

Nezames, C. D., Sjogren, C. A., Barajas, J. F., and Larsen, P. B. (2012). The *Arabidopsis* cell cycle checkpoint regulators TANMEI/ALT2 and ATR mediate the active process of aluminum-dependent root growth inhibition. Plant Cell 24(2), 608-621.

Orbach, R., and Howard, J. (2019) The dynamics and structural properties of axonemal tubulins support the high length stability of cilia. Nat. Commun. 10: 1838.

Olsen, J.L., Rouze, P., Verhelst, B., Lin, Y.C., Bayer, T., et al. (2016) The genome of the seagrass Zostera marina reveals angiosperm adaptation to the sea. Nature 530: 331-335.

Paredez, A.R., Somerville, C.R., and Ehrhardt, D.W. (2006) Visualization of cellulose synthase demonstrates functional association with microtubules. Science 312: 1491-1495.

Peng, J., Carol, P., Richards, D. E., King, K. E., Cowling, R. J., et al. (1997). The *Arabidopsis* GAI gene defines a signaling pathway that negatively regulates gibberellin responses. Genes Dev 11(23), 3194-3205.

Piperno, G., and Fuller, M. T. (1985). Monoclonal antibodies specific for an acetylated form of alpha-tubulin recognize the antigen in cilia and flagella from a variety of organisms. J. Cell Biol 101(6), 2085-2094.

Piperno, G., LeDizet, M., and Chang, X. J. (1987). Microtubules containing acetylated alpha-tubulin in mammalian cells in culture. J. Cell Biol 104(2), 289-302.

Prevo, B., Scholey, J.M., and JPeterman, E.J.G. (2017) Intraflagellar transport: mechanisms of motor action, cooperation, and cargo delivery. FEBS J. 284: 2905-2931.

Purton, S., and Rochaix, J. D. (1994). Complementation of a *Chlamydomonas reinhardtii* mutant using a genomic cosmid library. Plant Mol. Biol. 24(3), 533-537.

Pytela, J., Kato, T., and Hashimoto, T. (2010). Mitogen-activated protein kinase phosphatase PHS1 is retained in the cytoplasm by nuclear extrusion signal-dependent and independent mechanisms. Planta 231(6), 1311-1322.

Schiff, P. B., Fant, J., and Horwitz, S. B. (1979). Promotion of microtubule assembly in vitro by taxol. Nature 277(5698), 665.

Ramundo, S., Rahire, M., Schaad, O., and Rochaix, J. D. (2013). Repression of essential chloroplast genes reveals new signaling pathways and regulatory feedback loops in *Chlamydomonas*. Plant Cell 25(1), 167-186.

Robinson, D. R., Sherwin, T., Ploubidou, A., Byard, E. H., and Gull, K. (1995). Microtubule polarity and dynamics in the control of organelle positioning, segregation, and cytokinesis in the trypanosome cell cycle. J. Cell Biol. 128(6), 1163-1172.

Sagee, O., Goren, R., and Riov, J. (1980). Abscission of citrus leaf explants: Interrelationships of abscisic acid, ethylene, and hydrolytic enzymes. Plant Physiol. 66(4), 750-753.

Sakamoto, T., Inui, Y. T., Uraguchi, S., Yoshizumi, T., Matsunaga, S., et al. (2011). Condensin II alleviates DNA damage and is essential for tolerance of boron overload stress in *Arabidopsis*. Plant Cell 23(9), 3533-3546.

Schibler, M. J., and Huang, B. (1991). The colR4 and colR15 beta-tubulin mutations in *Chlamydomonas reinhardtii* confer altered sensitivities to microtubule inhibitors and herbicides by enhancing microtubule stability. J. Cell Biol. 113(3), 605-614.

Shetty, P., Gitau, M.M., and Maròti, G. (2019) Salinity stress responses and adaptation mechanisms in eukaryotic green microalgae. Cells 8: 1657.

Shimogawara, K., Fujiwara, S., and Usuda, H. (1998) High-efficiency transformation of *Chlamydomonas reinhardtii* by electroporation. Genetics 148: 1821-1828.

Siththisarn, S., Yokthongwattana, K., Mahong, B., Roytrakul, S., Paemanee, A., et al. (2017) Comparative proteomic analysis of *Chlamydomonas reinhardtii* control and a salinity-tolerant strain revealed by a differential protein expression pattern. Planta 246: 843-856.

Sjogren, C. A., Bolaris, S. C., and Larsen, P. B. (2015). Aluminum-dependent terminal differentiation of the *Arabidopsis* root tip is mediated through an ATR-, ALT2-, and SOG1-regulated transcriptional response. Plant Cell 27(9), 2501-2515.

Sorger, P. K., Dobles, M., Tournebize, R., and Hyman, A. A. (1997). Coupling cell division and cell death to microtubule dynamics. Curr. Opin. Cell Biol. 9(6), 807-814.

Spudich, J. L., and Sager, R. (1980). Regulation of the *Chlamydomonas* cell cycle by light and dark. J. Cell Biol. 85(1), 136-145.

Stecker, K.E., Minkoff, B.B., and Sussman, M.R. (2014) Phosphoproteomic analyses reveal early signaling events in the osmotic stress response. Plant Physiol. 165: 1171-1187.

Steinbacher, S., Hof, P., Eichinger, L., Schleicher, M., Gettemans, J., et al. (1999). The crystal structure of the *Physarum polycephalum* actin-fragmin kinase: an atypical protein kinase with a specialized substrate-binding domain. EMBO J. 18: 2923–2929.

Sugimoto, K., Williamson, R. E., and Wasteneys, G. O. (2000). New techniques enable comparative analysis of microtubule orientation, wall texture, and growth rate in intact roots of *Arabidopsis*. Plant Physiol. 124(4), 1493-1506.

Sun, T. P. (2011). The molecular mechanism and evolution of the GA–GID1–DELLA signaling module in plants. Curr. Biol. 21(9), R338-R345.

Suzuki, N., Miller, G., Salazar, C., Mondal, H. A., Shulaev, E., et al. (2013). Temporal-spatial interaction between reactive oxygen species and abscisic acid regulates rapid systemic acclimation in plants. Plant Cell 25(9), 3553-3569.

Tang, Q., Guittard-Crilat, E., Maldiney, R., Habricot, Y., Miginiac, E., et al. (2016). The mitogen-activated protein kinase phosphatase PHS1 regulates flowering in *Arabidopsis thaliana*. Planta 243(4), 909-923.

Theodosiou, A., and Ashworth, A. (2002) MAP kinase phosphatases. Genome Biol. 3: 3009.

Tietel, Z., Wikoff, W.R., Kind, T., Ma, Y., and Fiehn, O. (2020) Hyperosmotic stress in *Chlamydomonas* induces metabolomics changes in biosynthesis of complex lipids. Eur. J. Phycol. 55: 11-29.

Toso, R. J., Jordan, M. A., Farrell, K. W., Matsumoto, B., and Wilson, L. (1993). Kinetic stabilization of microtubule dynamic instability in vitro by vinblastine. Biochem 32(5), 1285-1293.

Tulin, F., and Cross, F.R. (2014) A microbial avenue to cell cycle control in the plant superkingdom. Plant Cell 26: 4019-4038.

Tulin, F., and Cross, F. R. (2015). Cyclin-dependent kinase regulation of diurnal transcription in *Chlamydomonas*. Plant Cell 27(10), 2727-2742.

Tuteja, N., and Mahajan, S. (2007). Calcium signaling network in plants: an overview. Plant Signal. Behav 2(2), 79-85.

Ueki, N., Ide, T., Mochiji, S., Kobayashi, Y., Tokutsu, R., et al. (2016). Eyespot-dependent determination of the phototactic sign in *Chlamydomonas reinhardtii*. PNAS 113(19), 5299-5304.

Umen, J.G. (2018) Sizing up the cell cycle: systems and quantitative approaches in *Chlamydomonas*. Curr. Opin. Plant Biol. 46: 96-103.

Umezawa, T., Sugiyama, N., Takahashi, F., Anderson, J. C., Ishihama, Y., et al. (2013). Genetics and phosphoproteomics reveal a protein phosphorylation network in the abscisic acid signaling pathway in *Arabidopsis thaliana*. Sci. Signal 6(270), rs8-rs8.

Van de Weghe, J.C., Harris, J.A., Kubo, T., Witman, G.B., and Lechtreck, K.F. (2020) Diffusion rather than intraflagellar transport likely provides most of the tubulin required for axonemal assembly in *Chlamydomonas*. J. Cell Sci. 133: jcs249805.

Van Damme, D., Van Poucke, K., Boutant, E., Ritzenthaler, C., Inzé, D., et al. (2004). In vivo dynamics and differential microtubule-binding activities of MAP65 proteins. Plant Physiol 136(4), 3956-3967.

Valledor, L., Furuhashi, T., Hanak, A. M., and Weckwerth, W. (2013). Systemic cold stress adaptation of *Chlamydomonas reinhardtii*. Mol. Cell Proteomics, 12(8), 2032-2047.

Verslues, P. E., Agarwal, M., Katiyar-Agarwal, S., Zhu, J., and Zhu, J. K. (2006). Methods and concepts in quantifying resistance to drought, salt and freezing, abiotic stresses that affect plant water status. Plant J. 45(4), 523-539.

Vinocur, B., and Altman, A. (2005). Recent advances in engineering plant tolerance to abiotic stress: achievements and limitations. Curr. Opin. Biotechnol. 16(2), 123-132.

Wang, C., Li, J., and Yuan, M. (2007). Salt tolerance requires cortical microtubule reorganization in *Arabidopsis*. Plant Cell Physiol. 48(11), 1534-1547.

Wang, C., Liu, Y., Li, S. S., and Han, G. Z. (2015). Insights into the origin and evolution of the plant hormone signaling machinery. Plant Physiol. 167(3), 872-886.

Wang, N., Qian, Z., Luo M., Fan, S. Zhang, X. et al. (2018) Identification of salt stress responding genes using transcriptome analysis in green algae *Chlamydomonas reinhardtii*. Int. J. Mol. Sci. 19: 3359.

Webster, D. R., and Borisy, G. G. (1989). Microtubules are acetylated in domains that turn over slowly. J. Cell Sci. 92(1), 57-65.

Werth, E.G., McConnell, E.W., Gilbert, T.S.K., Lianez, I.C., Perez, C.A., et al. (2017) Probing the global kinome and phosphoproteome in *Chlamydomonas reinhardtii* via sequential enrichment and quantitative proteomics. Plant J. 89: 416-426.

Whittington, A. T., Vugrek, O., Wei, K. J., Hasenbein, N. G., Sugimoto, K., et al. (2001). MOR1 is essential for organizing cortical microtubules in plants. Nature 411(6837), 610-613.

Witman, G. (2009) The *Chlamydomonas* Sourcebook, Volume 2. Chapter 2; Basal bodies and associated structures, Elsevier, Oxford, pp. 15-42.

Wodniok, S., Brinkmann, H., Glöckner, G., Heidel, A. J., Philippe, H., Melkonian, M., and Becker, B. (2011). Origin of land plants: do conjugating green algae hold the key?. BMC Evol. Biol. 11(1), 104.

Xiao, H., Verdier-Pinard, P., Fernandez-Fuentes, N., Burd, B., Angeletti, R., et al. (2006). Insights into the mechanism of microtubule stabilization by Taxol. PNAS 103(27), 10166-10173.

Xiong, L., and Zhu, J. K. (2002). Molecular and genetic aspects of plant responses to osmotic stress. Plant Cell Environ. 25(2), 131-139.

Xu, Z., Schaedel, L, Portran, D., Aguilar, A., Gaillard, J., et al. (2017) Microtubules acquire resistance from mechanical breakage through intraluminal acetylation. Science 356: 328-332.

Yamano, T., Iguchi, H., and Fukuzawa, H. (2013). Rapid transformation of *Chlamydomonas reinhardtii* without cell-wall removal. J. Biosci. Bioeng. 115(6), 691-694.

Yoshiyama, K. O., Kimura, S., Maki, H., Britt, A. B., and Umeda, M. (2014). The role of SOG1, a plant-specific transcriptional regulator, in the DNA damage response. Plant Signal Behav. 9(4), e28889.

Yoshiyama, K. O. (2015). SOG1: a master regulator of the DNA damage response in plants. Genes Genet. Syst. 90(4), 209-216.

Yoshiyama, K., Conklin, P. A., Huefner, N. D., and Britt, A. B. (2009). Suppressor of gamma response 1 (SOG1) encodes a putative transcription factor governing multiple responses to DNA damage. PNAS 106(31), 12843-12848.

Yasumura, Y., Crumpton-Taylor, M., Fuentes, S., and Harberd, N. P. (2007). Step-by-step acquisition of the gibberellin-DELLA growth-regulatory mechanism during land-plant evolution. Curr. Biol. 17(14), 1225-1230.

Zhu, J. K. (2002). Salt and drought stress signal transduction in plants. Annu. Rev. Plant Biol. 53(1), 247-273.